Acta Biomaterialia xxx (xxxx) xxx

Contents lists available at ScienceDirect

Acta Biomaterialia

journal homepage: www.elsevier.com/locate/actabiomat

Full length article

Oxidized alginate hydrogels with the GHK peptide enhance cord blood mesenchymal stem cell osteogenesis: A paradigm for metabolomics-based evaluation of biomaterial design

Michail E. Klontzas [a], Supachai Reakasame [b], Raquel Silva [b], Jose C.F. Morais [a], Spyros Vernardis [a], Robert J. MacFarlane [a], Manolis Heliotis [c], Eleftherios Tsiridis [d], Nicki Panoskaltsis [e,f], Aldo R. Boccaccini [b], Athanasios Mantalaris [a,*]

[a] Biological Systems Engineering Laboratory, Department of Chemical Engineering & Chemical Technology, Imperial College London, London, UK
[b] Institute of Biomaterials, Department of Materials Science and Engineering, University of Erlangen-Nuremberg, Erlangen, Germany
[c] Department of Oral and Maxillofacial Surgery, Northwick Park Hospital, London North West University Healthcare NHS Trust, London, UK
[d] Academic Orthopaedic Unit, Aristotle University Medical School, Thessaloniki, Greece
[e] Department of Hematology, Imperial College London, London, UK
[f] Winship Cancer Institute, Department of Hematology & Medical Oncology, Emory University, Atlanta, GA, USA

ARTICLE INFO

Article history:
Received 5 December 2018
Received in revised form 8 February 2019
Accepted 13 February 2019
Available online xxxx

Keywords:
Metabolomics
Metabolism
Hydrogels
GHK
Mesenchymal stem cells
Osteogenic differentiation

ABSTRACT

Oxidized alginate hydrogels are appealing alternatives to natural alginate due to their favourable biodegradability profiles and capacity to self-crosslink with amine containing molecules facilitating functionalization with extracellular matrix cues, which enable modulation of stem cell fate, achieve highly viable 3-D cultures, and promote cell growth. Stem cell metabolism is at the core of cellular fate (proliferation, differentiation, death) and metabolomics provides global metabolic signatures representative of cellular status, being able to accurately identify the quality of stem cell differentiation. Herein, umbilical cord blood mesenchymal stem cells (UCB MSCs) were encapsulated in novel oxidized alginate hydrogels functionalized with the glycine-histidine-lysine (GHK) peptide and differentiated towards the osteoblastic lineage. The ADA-GHK hydrogels significantly improved osteogenic differentiation compared to gelatin-containing control hydrogels, as demonstrated by gene expression, alkaline phosphatase activity and bone extracellular matrix deposition. Metabolomics revealed the high degree of metabolic heterogeneity in the gelatin-containing control hydrogels, captured the enhanced osteogenic differentiation in the ADA-GHK hydrogels, confirmed the similar metabolism between differentiated cells and primary osteoblasts, and elucidated the metabolic mechanism responsible for the function of GHK. Our results suggest a novel paradigm for metabolomics-guided biomaterial design and robust stem cell bioprocessing.

Statement of Significance

Producing high quality engineered bone grafts is important for the treatment of critical sized bone defects. Robust and sensitive techniques are required for quality assessment of tissue-engineered constructs, which result to the selection of optimal biomaterials for bone graft development. Herein, we present a new use of metabolomics signatures in guiding the development of novel oxidised alginate-based hydrogels with umbilical cord blood mesenchymal stem cells and the glycine-histidine-lysine peptide, demonstrating that GHK induces stem cell osteogenic differentiation. Metabolomics signatures captured the enhanced osteogenesis in GHK hydrogels, confirmed the metabolic similarity between differentiated cells and primary osteoblasts, and elucidated the metabolic mechanism responsible for the function of GHK. In conclusion, our results suggest a new paradigm of metabolomics-driven design of biomaterials.

* Corresponding author at: BioMedical Systems Engineering Laboratory, Wallace H. Coulter Department of Biomedical Engineering, Georgia Institute of Technology, 950 Atlantic Drive, Engineering Biosciences Building, Rm 3016, Atlanta, GA 30332, USA.
E-mail address: sakis.mantalaris@gatech.edu (A. Mantalaris).

https://doi.org/10.1016/j.actbio.2019.02.017
1742-7061/

1. Introduction

Alginate hydrogels have been extensively utilized as tissue engineering materials because of their low cost, abundance in nature, biocompatibility, malleability and ability to gelate under conditions that cause minimal cell stress [1]. However, the absence of alginate-degrading enzymes in mammals limits the *in vivo* degradability of natural alginate. In addition, the lack of cell-interacting regions on the structure of alginate reduces cell adhesion and requires developing strategies to promote attachment and cellular infiltration within the alginate hydrogels [2]. In order to overcome these limitations, oxidized alginate (alginate di-aldehyde; ADA) has been employed as an attractive alternative [3,4]. The free aldehyde groups of ADA can form covalent bonds with molecules that contain amino groups (such as proteins or small peptides) enabling the crosslinking with bioactive substances that can modulate stem cell physiology [5–8].

Gelatin is widely used to promote cell adhesion in alginate hydrogels and can be crosslinked to ADA or natural alginate in order to increase its stability. ADA-gelatin hydrogels have been employed in a variety of tissue engineering applications, including cardiac, bone, cartilage, vessel, corneal, liver and muscle tissue engineering, as well as in wound healing and tissue fixation [4]. Sarker et al. have developed a cell-friendly method to produce ADA hydrogels crosslinked with gelatin (ADA-Gel) at pH = 7.4 with the use of phosphate buffered saline (PBS) [8–10]. The resulting hydrogels have excellent biocompatibility, enhanced degradation properties, increased stability of gelatin in culture, and promote cell adhesion while also being good candidates for 3D printing applications [11]. Apart from gelatin, other proteins or peptides have been used to provide extracellular matrix cues in alginate hydrogels, primarily collagen and the arginyl-glycyl-aspartic acid (RGD) peptide [12,13]. The glycine-histidine-lysine (GHK) peptide is a fragment of osteonectin (SPARC), a protein abundant in bone extracellular matrix. GHK promotes secretion of vascular endothelial growth factor (VEGF) and basic fibroblast growth factor (bFGF) from mesenchymal stem cells (MSCs) in alginate hydrogels, increasing stem cell proliferation and promoting secretion of collagen, elastin and other factors related to wound healing [14–16]. The GHK-copper (GHK-Cu) complex has been previously covalently crosslinked with natural alginate in an attempt to increase the proangiogenic potential of bone marrow MSCs [14]. However, it has been suggested that it is not GHK-Cu, but copper-free GHK that exerts positive effects on osteoblasts, as indicated by the fact that GHK-Cu inhibited osteoblastic alkaline phosphatase (ALP) activity and osteocalcin secretion [17], whereas collagen gels loaded with copper-free GHK accelerated healing in guinea-pig bone defects [15]. Consequently, biomaterial functionalisation with GHK could prove beneficial in bone tissue engineering applications; however, the effect of copper-free GHK on the osteogenic differentiation of human MSCs remains to be determined.

Umbilical cord blood mesenchymal stem cells (UCB MSCs) have been used in bone tissue engineering for their superior immunosuppressive properties and enhanced proliferation capacity compared to their adult equivalents, specifically bone marrow and adipose MSCs [18–20]. Sourcing MSCs from umbilical cord blood units stored in blood banks offers the potential for off-the-shelf bone graft production, meeting clinical demands and avoiding the limitations associated with the use of autografts and allografts [20]. UCB MSCs have been shown to be at least equal to bone marrow MSCs in generating bone when implanted in mice and have been characterized as circulating fetal chondro-osteoprogenitors contributing to skeletal development [21].

Metabolomics analysis enables the simultaneous identification and quantification of all measurable small metabolites (<1 kDa) within a cell, providing a global assessment of the cellular metabolic state. Alterations in the genomic, transcriptomic and proteomic landscape and environmental perturbations are dynamically accompanied by changes in metabolic pathway activities, rendering metabolism the level of cellular function that most accurately reflects cellular phenotype [22,23]. Metabolomics has been used as a high-throughput platform for the evaluation of mammalian cell physiology [24,25] and holds great potential for cell culture engineering due its high sensitivity and low operating costs compared to other omics platforms [26]. It can manifest the degree of osteogenic differentiation in 2D cultures [27], has been used to detect osteoinductive molecules in hydrogels with variable stiffness [28] and has been applied to the detection of pathways activated in skeletal stem cells when exposed to nanotopographical cues [29,30] and in cancer cells responding to polymers conjugated with chemotherapeutic agents [31]. Apart from the widespread use of metabolomics for the evaluation of pathway activities and the elucidation of complex molecular mechanisms, it can also produce global cell state-specific metabolic signatures [24,32]. Such metabolomics-derived signatures have been used for monitoring and quality control of mammalian cell cultures [33] but have not yet been used for the assessment of 3D stem cell cultures in biomaterials. It has been recently suggested that omics approaches, such as metabolomics, should be utilized to assess therapeutic MSC potency given the ambiguity regarding MSC functions and origin, and the rise of unapproved stem cell treatment marketing [34]. Consequently, metabolomics sensitivity and the dynamic nature of metabolic changes in response to intracellular and extracellular cues [33] can be exploited for the high-resolution assessment of tissue engineered products with potential clinical applications.

Herein, we present the development of a novel hydrogel consisting of ADA and copper-free GHK, which was seeded with UCB MSCs to evaluate its suitability in bone tissue engineering applications. The hydrogel was produced according to the non-cytotoxic method of Sarker et al. [8], combining the optimal biodegradability of oxidized alginate and providing an alternative to the use of animal-derived gelatin which can transmit pathogens and trigger undesirable immune responses when implanted *in vivo*. Our work is the first to demonstrate the capacity of GHK to promote MSC osteogenic differentiation. UCB MSCs were selected for encapsulation within the hydrogels due to their higher proliferation capacity compared to other MSC types, potential for off-the-shelf use, and their inherent commitment to the osteogenic and chondrogenic lineages [21]. The ADA-GHK hydrogels were compared to the gelatin-containing hydrogels controls (ADA-Gel, ADA-Gel-GHK) demonstrating that GHK enhanced viability, proliferation and osteogenic differentiation. Metabolomics signatures were utilized at several steps of the biomaterial development process, revealing the effects of hydrogel composition on UCB MSC phenotype, demonstrating the superior osteogenic capacity of GHK-containing hydrogels, and elucidating the mechanism of GHK action, which was related to integrin b1 and mediated by integrin linked kinase (ILK). The importance of our results is: (1) the development of a cell-laden biomaterial that enhances osteogenesis and combines the advantages of UCB MSCs, GHK and oxidized alginate with potential applications in bone tissue engineering, and (2) the potential utilisation of metabolomics profiles as quality control signatures of osteogenesis, which can inform the design of biomaterials.

2. Materials & methods

2.1. Hydrogel fabrication

ADA was produced according to previous methods [8]. Briefly, 50 mL of 20% w/v sodium alginate in ethanol (MW

Please cite this article as: M. E. Klontzas, S. Reakasame, R. Silva et al., Oxidized alginate hydrogels with the GHK peptide enhance cord blood mesenchymal stem cell osteogenesis: A paradigm for metabolomics-based evaluation of biomaterial design, Acta Biomaterialia, https://doi.org/10.1016/j.actbio.2019.02.017

100,000–200,000 g/mol, 65–70% guluronic acid, Sigma-Aldrich, UK) was oxidized with 2.674 g of sodium metaperiodate dissolved in 50 mL of deionized water for 6 h in the dark and the reaction was quenched with the addition of ethylene glycol (10 mL) (VWR, UK). Removal of metaperiodate was achieved by dialysis in ultrapure water in a 6000–8000 Da MWCO dialysis membrane (SpectrumLab, USA), with twice-a-day water replacements for one week, yielding ADA with a degree of oxidation of 33% [8]. Clearance of metaperiodate was confirmed with the addition of 0.5 mL of 1% w/v silver nitrate to 5 mL of the dialysate at the final day of the experiment. Absence of precipitation confirmed the total elimination of metaperiodate from the ADA solution, which was frozen in −20 °C and freeze-dried. ADA allows for the self-crosslinking of molecules with free amine groups, such as proteins and peptides, offering a stable alternative to blending [4]. Consequently, ADA was used to construct three types of hydrogels, ADA with gelatin (ADA-Gel), ADA with GHK (ADA-GHK), and ADA with both gelatin and GHK (ADA-Gel-GHK). The final concentration of ADA and gelatin in all hydrogels was 3% and 2% w/v, respectively. GHK was used at a concentration of 0.5% w/v following optimisation of viability, cell numbers and alkaline phosphatase activity (data not shown). GHK used in this study was synthesized in a copperless form (H-GGGGGHKSP-OH, Mimotopes Ltd., UK). All solutions were filter-sterilized prior to cell encapsulation.

2.2. UCB MSC encapsulation and culture

Fetal MSCs were isolated from umbilical cord blood according to previous methods [20,27], with the mothers' informed consent and according to the corresponding ethical approval (05/Q0405/20; NRES Committee, London, Harrow, UK). Cells were expanded until passage 5 at 37 °C, 5% CO_2, 21% O_2 in αMEM Glutamax-I with 10% FBS and 1% penicillin-streptomycin (proliferation medium). Cells were gently mixed with hydrogel solutions at a concentration of 2×10^6 cells/mL and incubated for 2 min in 37 °C in order to facilitate ADA conjugation with gelatin and GHK. The cell-hydrogel suspension was passed through a peristaltic pump leading to a 25-gauge needle. Beads were extruded through the needle to a 100 mM $CaCl_2$ and 10 mM HEPES buffer (pH = 7.4) where they underwent crosslinking for 10 min. Subsequently, beads were washed in PBS and cultured in proliferation medium for 3 days to permit cell adaptation to the 3D environment. After 3 days, osteogenesis was induced by supplementing the proliferation medium with 10^{-7} M dexamethasone, 50 μg/mL ascorbic acid 2-phosphate and 10 mM β-glycerophosphate (osteogenic medium). Medium was replenished every two days for three weeks and samples were collected at day 7, 14 and 21.

2.3. Cell viability analysis

Cell viability in hydrogels was assessed with the use of LIVE/DEAD viability assay (Life Technologies, UK). Samples were collected, washed in PBS and incubated for 1 h in a solution of 2 μM calcein AM (staining live cells) and 4 μM ethidium homodimer-1 (staining dead cells). Images were captured in a Leica SP5 (Leica Microsystems, UK) inverted confocal microscope using a 512 × 512 pixel resolution, 10x magnification and a slice thickness of 10 μm. Quantification of live and dead cells was performed on the captured images using the 3D Object Counter plugin of Fiji [35,36] utilising the same number of slices across all groups. Live/dead images were prepared as maximal intensity Z-stack projections. After quantification and solely for presentation purposes, brightness and contrast have been adjusted equally for all groups.

2.4. GHK stability in ADA hydrogels

A custom FITC-labelled GHK peptide (Mimotopes Ltd., UK) was used to confirm whether GHK was retained within the hydrogels for the duration of the culture. FITC was attached to a lysine residue away from the $-NH_2$ end of the peptide, allowing the possible self-conjugation of GHK to ADA. Specifically, cell-free hydrogels (N = 3) were fabricated using the FITC-labelled peptide and cultured in proliferation medium for 24 days. Images were captured using a Leica Inverted Fluorescent Microscope (Leica Microsystems, UK) at day 0, 3, 10, 17 and 24 and hydrogels with unlabelled GHK were used as negative controls. Release of GHK in culture medium was quantified by culturing cell-free ADA-GHK hydrogels in α-MEM without the addition of FBS (3 beads in 1 mL of culture medium). Supernatants (N = 3) were collected at days 0, 3, 10, 17 and 24 and peptide concentration was measured with the use of Micro BCA protein assay kit according to manufacturer's instructions (ThermoFisher, UK). Micro BCA can detect peptide concentrations as low as 0.5 μg/mL, which is sensitive enough for the detection of minimal GHK release by ADA-GHK hydrogels. Consequently, concentrations less than 0.5 μg/mL were considered undetected and assigned a value of 0. Briefly, 150 μL of supernatant were incubated with 150 μL of Micro BCA working solution for 2 h at 37 °C in the dark and absorbance was measured at 562 nm using a Promega Reader (Promega GloMax, Promega, UK). Blank supernatant fluorescence was subsequently subtracted and GHK concentrations were calculated using a standard curve constructed using albumin standards.

2.5. DNA quantification

The quantity of DNA in alginate beads was used as a measure of cell number for metabolomics and ALP activity normalisation, as reported in previous work [27,37]. Alginate beads of each group (N = 3) were collected, washed with PBS, and incubated overnight at 50 °C in dissolution/digestion buffer containing 10 mM Tris – 1 mM EDTA buffer with 0.1% v/v Triton-X (Sigma, UK) and 0.1 mg/mL Proteinase K (Life Technologies, UK). The resulting solution was dissolved 1:10 in PBS and DNA was quantified using the Quant-it PicoGreen assay (ThermoFisher, UK) by incubating 100 μL of DNA solution with 100 μL of PicoGreen working solution for 5 min in the dark and measuring fluorescence at 485 nm/530 nm of excitation/emission wavelengths. Finally, cell numbers were calculated with a standard curve constructed with UCB MSCs. DNA quantification cannot discriminate against the presence of dead cells in the hydrogels but represents a suitable technique available for the normalisation of metabolomics data from adherent cultures [48].

2.6. Alkaline phosphatase activity

ALP activity was quantified as an indirect measure of osteogenic differentiation. Beads of each experimental group (N = 3) were collected, washed with PBS and incubated with 50:50 alkaline buffer solution (Sigma, UK):pNPP substrate (Sigma, UK) at 37 °C in the dark for 30 min. The reaction was terminated with equal volume 0.5 N NaOH and absorbance was measured at 405 nm. Results were normalized using the cell numbers derived from DNA quantification (described above) and ALP activity was expressed as pNPP/min/10^6 cells using a pNPP standard curve.

2.7. Fourier-Transform Infrared Spectroscopy (FTIR)

The quality of the mineralized matrix produced in different hydrogels was assessed by means of Fourier-transform infrared spectroscopy. Beads were collected, washed three times with

Please cite this article as: M. E. Klontzas, S. Reakasame, R. Silva et al., Oxidized alginate hydrogels with the GHK peptide enhance cord blood mesenchymal stem cell osteogenesis: A paradigm for metabolomics-based evaluation of biomaterial design, Acta Biomaterialia, https://doi.org/10.1016/j.actbio.2019.02.017

ultrapure water, frozen at −80 °C and freeze-dried in an ethylene glycol bath (−15 °C). FTIR data collection was performed with a Spectrum 100 FTIR instrument (Perkin Elmer, UK). For every sample, 16 scans were recorded with a resolution of 2 cm^{-1} between 900 and 4000 cm^{-1}. The mineral-to-matrix ratio (MM_r) was calculated on the baseline corrected spectra as previously described [38–40], by dividing the area under the curve of phosphate bands (900–1200 cm^{-1}) by the area under the curve of amide I bands (1585–1725 cm^{-1}). Experiments were run in triplicates and representative samples were selected to demonstrate the quality of matrix mineralisation in different groups.

2.8. Real time quantitative RT-PCR

Hydrogel beads were collected at day 0 and day 21 of osteogenic differentiation and RNA was extracted with the use of RNeasy Mini Kit (Qiagen, UK) according to the protocol provided by the manufacturer. qRT-PCR was performed with the KAPA SYBR FAST One-Step ABI PRISM Kit (Sigma-Aldrich, UK), in an ABI StepOnePlus PCR instrument (ThermoFisher, UK) with the cycling protocol described elsewhere [27]. Gene expression of *Runt-related transcription factor 2* (*Runx2*), *osteocalcin* (*OCN*), *collagen type IA1* (*Col 1A1*), *integrin β1* and *integrin linked kinase* (*ILK*) was assessed with the primers presented in Table 1 [41–46]. *RPL13a* was used as the housekeeping gene and results were analysed with the $2^{-\Delta\Delta Ct}$ method [47] relative to the expression of ADA-Gel at each time point.

2.9. Immunofluorescence

Protein levels before and after UCB MSC osteogenic differentiation were assessed by means of double immunofluorescence with confocal microscopy. Briefly, alginate beads were washed in PBS and fixed overnight in 4% w/v paraformaldehyde. Samples were permeabilized in 0.1% v/v Triton-X 100, blocked with 10% v/v donkey serum in PBS and incubated overnight with primary antibodies against Col IA1 and OCN or integrin β1 and ILK. Alexa Fluor 488 and Alexa Fluor 647 secondary antibodies were used to label Col IA1 and OCN or integrin β1 and ILK respectively and samples were counterstained with 4,6-diamidino-phenylindole (DAPI, 1:1000 in PBS). Secondary antibody controls were used to assess non-specific staining of the secondary antibody. Details about the antibodies and the setup of immunofluorescence experiments can be found in Table 2.

Images of immunofluorescence experiments were captured in a Leica SP5 inverted confocal microscope using a 512 × 512 pixel resolution, 10× magnification and a section thickness of 10 μm. For each image comparison, the same number of slices of a representative stack from each group (surface to core) has been used for image reconstruction. Brightness and contrast were equally adjusted in all images for presentation purposes maintaining all the features of the originals. Maximal projection Z-stacks were prepared with Fiji image analysis software [36].

2.10. GC–MS metabolomics & bioinformatics analysis

Metabolomics analysis of encapsulated UCB MSCs was performed as previously described [24,27] with a protocol adapted to 3D hydrogel cultures. Specifically, hydrogels (N = 10) from each group were collected, washed with PBS and metabolism was quenched by liquid nitrogen snap-freezing. Hydrogels were grinded with a mortar and pestle and the resulting powder was dissolved in ice cold methanol. Extraction of metabolites was performed according to Kanani et al. [26]. Ribitol (1 mg/10^6 cells) was added to the metabolite mixture as an internal standard and ^{13}C-glucose (2 mg/10^6 cells) was used to validate the robust operation conditions of mass spectrometry [26]. DNA quantification results were used for normalisation purposes [27,48]. Dried polar metabolite mixtures were derivatized for 1.5 h in 50 μL Methoxyamine hydrochloride (MeOx, Sigma, UK) followed by 6 h derivatisation in 100 μL N-methyl-trimethylsylyl – trifluoroacetamide (MSTFA, Alfa Aesar, UK) and samples were run in quadruplicates in a Shimadzu QP2010 Ultra Gas Chromatography – Mass Spectrometry (GC–MS) instrument (Shimadzu, UK).

Data preparation was accomplished based on Kanani & Klapa [49] and relative peak areas of consistently quantified metabolites (CV < 25% between technical quadruplicates) were calculated with regards to the peak area of the marker ion 103 of ribitol. Bioinformatics analysis of the resulting dataset was performed in R (v. 3.4.2, https://www.R-project.org/) on z-scores of the relative peak areas in an unsupervised manner, employing Principal Component Analysis (PCA) and Hierarchical clustering with Manhattan distance metric. Hierarchical clustering of heatmap profiles is a fundamental machine learning strategy, widely utilized to provide unbiased information regarding similarity of multidimensional metabolic signatures, rather than an objective evaluation of heatmap colours [50]. Statistical analysis of multidimensional metabolomics data was performed with Significance Analysis for Microarrays (SAM) in TM4 MeV (v. 4.9.0) [51] with a median- false discovery rate (FDR) set to 0%. Significantly increased or decreased metabolites were presented on a reconstruction of the core metabolic network of UCB MSCs as previously published [27]. Metabolomics profiles of primary osteoblasts were sourced

Table 1
Primers used in real-time qRT-PCR.

Gene	Forward Primer	Reverse Primer	References
Runt-related transcription factor 2 (*Runx2*)	5′-GAGGTACCAGATGGGACTGTG-3′	5′-TCGTTGAACCTTGCTACTTGG-3′	[42]
Osteocalcin (*OCN*)	5′-GGCAGCGAGGTAGTGAAGAG-3′	5′-CTCACACACCTCCCTCCT-3′	[43]
Collagen type IA1 (*Col 1A1*)	5′-TGACCTCAAGATGTGCCACT-3′	5′-ACCAGACATGCCTCTTGTCC-3′	[44]
Integrin linked kinase (*ILK*)	5′-ACCAGACATGCCTCTTGTCC-3′	5′-ACCTCTGGAGTTCAGGCAAGG-3′	[45]
Integrin β1	5′-GTGAGTGCAACCCCAACTACAC-3′	5′- TGTCCGTTGCTGGCTTCA-3′	[45]
Ribosomal Protein L13a (RPL13a)	5′-CTATGACCAATAGGAAGAGCAACC-3′	5′-GCAGAGTATATGACCAGGTGGAA-3′	[46,47]

Table 2
Antibodies used for immunofluorescence.

Antigen	Blocking	Primary antibody	Secondary Antibody	Company
Collagen I A1	Donkey serum	Mouse monoclonal (3 μg/mL)	Donkey Anti-Mouse IgG AF 488 (1:200 dilution)	Abcam
Osteocalcin		Rabbit polyclonal (5 μg/mL)	Donkey Anti-Rabbit IgG AF 647 (1:200 dilution)	
Integrin β1		Mouse monoclonal (10 μg/mL)	Donkey Anti-Mouse IgG AF 488 (1:200 dilution)	
Integrin Linked Kinase (ILK)		Rabbit monoclonal (1:100 dilution)	Donkey Anti-Rabbit IgG AF 647 (1:200 dilution)	

Please cite this article as: M. E. Klontzas, S. Reakasame, R. Silva et al., Oxidized alginate hydrogels with the GHK peptide enhance cord blood mesenchymal stem cell osteogenesis: A paradigm for metabolomics-based evaluation of biomaterial design, Acta Biomaterialia, https://doi.org/10.1016/j.actbio.2019.02.017

from previous work in our group [27] and compared to the profiles of undifferentiated and terminally differentiated MSCs in all hydrogel groups.

2.11. Integrin linked kinase inhibition

ILK activity was inhibited with the use of CPD22 (Calbiochem, USA) at 1 μM as previously described [52,53]. CPD22 is specific for ILK and 1 μM has been found to completely inhibit ILK activity without impairing the function of mononuclear [52] and epithelial cells [53]. Mediation of GHK actions by ILK was assessed by culturing UCB MSCs in the presence, absence or combination of GHK and CPD22 (Supplementary Table 1). Cells were rested for 12 h after encapsulation and then CPD22-suplemented proliferation medium was applied for 48 h. At 60 h post encapsulation (following recovery from the stress of encapsulation and prior to the initiation of

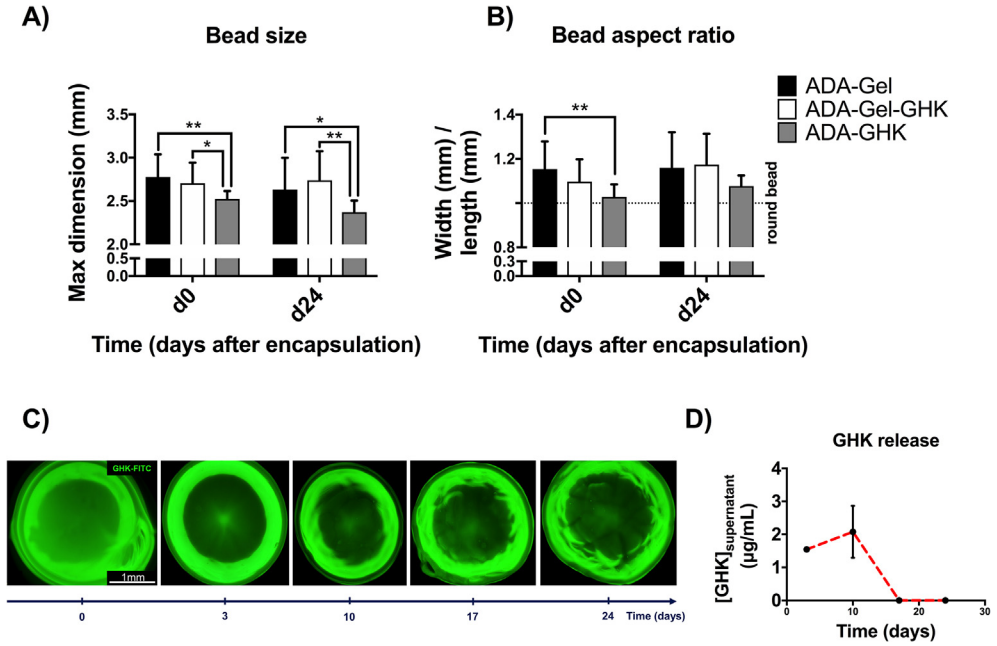

Fig. 1. Structural characteristics of alginate beads. Maximum dimension (A) and aspect ratio (B) comparison over 24 days in culture. Bars represent mean ± SD (N = 10–15 beads). The dashed line represents the aspect ratio of round beads. FITC-labelled GHK beads (C) demonstrating the presence of GHK in hydrogels over 24 days. Controls with unlabeled GHK have been used to set the fluorescence threshold. Release of GHK as quantified in supernatants collected from 3 beads (N = 3) (D). d0: day 0 after encapsulation; d24: day 24 after encapsulation; Scale bar = 1 mm; * P < 0.05; ** P < 0.01.

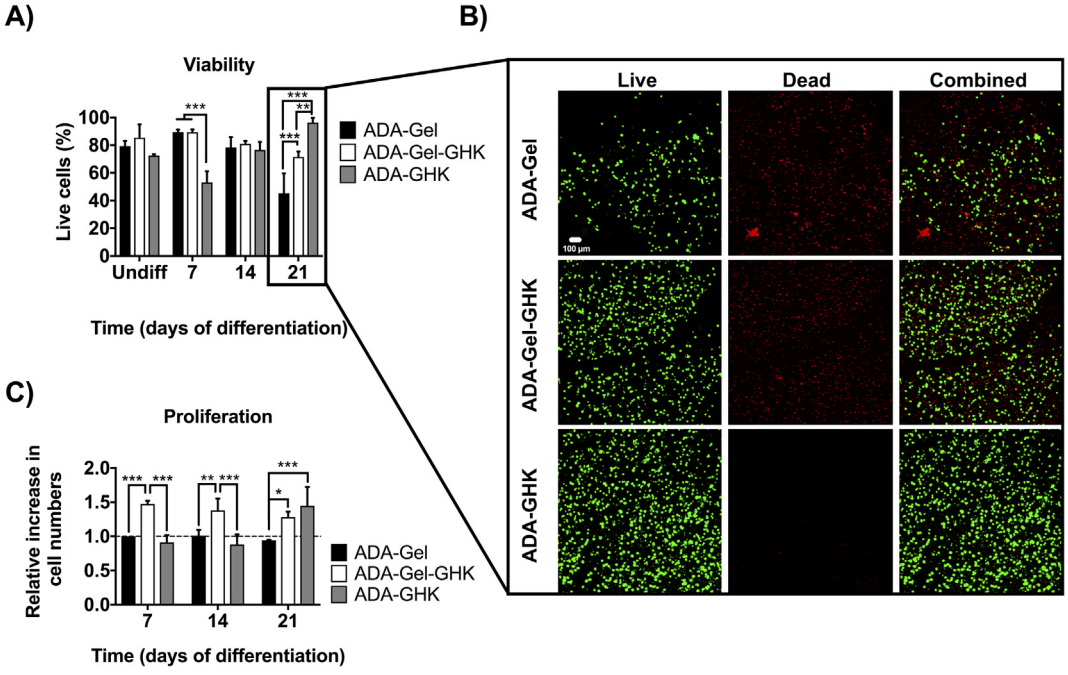

Fig. 2. Cell viability and proliferation during osteogenic differentiation. Cell viability has been assessed by quantifying calcein AM (live) and EthD-1(dead) staining before the start and over the course of differentiation (N = 3) (A). Representative images of live (green) and dead (red) cells are shown at the end of differentiation (B). Proliferation relative to day 7 ADA-Gel has been assessed by means of DNA quantification (C). Bars represent mean ± SD (N = 3); Scale bar = 100 μm; * P < 0.05; ** P < 0.01; *** P < 0.001. (For interpretation of the references to color in this figure legend, the reader is referred to the web version of this article.)

Please cite this article as: M. E. Klontzas, S. Reakasame, R. Silva et al., Oxidized alginate hydrogels with the GHK peptide enhance cord blood mesenchymal stem cell osteogenesis: A paradigm for metabolomics-based evaluation of biomaterial design, Acta Biomaterialia, https://doi.org/10.1016/j.actbio.2019.02.017

differentiation) Live/Dead quantification, DNA quantification, and metabolomics analysis were performed to evaluate the involvement of ILK in GHK induced proliferation and metabolism.

2.12. Statistical analysis

Data were expressed as mean ± standard deviation and univariate data analysis was performed with the use of GraphPad Prism 7.0c for Mac OS X (GraphPad Software Inc., La Jolla, California, USA). Group means were compared with one-way (in cases with one independent variable) or two-way ANOVA (in cases with two independent variables) and Tukey's post-hoc test with significance set at a = 0.05 (N = 3 independent biological replicates, n = 3 technical replicates, unless stated otherwise).

3. Results

3.1. Hydrogel shape, size and peptide stability in culture

ADA-GHK hydrogels were smaller than ADA-Gel ($P = 0.006$ and $P = 0.02$ for day 0 and day 24, respectively) and ADA-Gel-GHK ($P = 0.04$ and $P = 0.001$ for day 0 and day 24, respectively), as shown in Fig. 1A. Immediately following encapsulation, the aspect ratio of ADA-GHK beads was lower than that of ADA-Gel beads ($P = 0.002$). However, at the end of the 24 day period no statistically significant difference was observed in the aspect ratio between the three groups (Fig. 1B). Analysis of GHK-FITC-labelled hydrogels confirmed that GHK remained within the hydrogel matrix throughout the culture period (Fig. 1C). This result was also supported by minimal release of GHK in the culture medium, which was detectable in concentrations of approximately 2 μg/mL only until about day 10 (Fig. 1D). From day 17 onwards the peptide was not detected.

3.2. GHK increases cell viability and proliferation

Viability was assessed by means of Live/Dead staining and quantification. Prior to the initiation of differentiation, viability was similar in all experimental groups (approximately 80%). Viability declined in the first 7 days of differentiation in the ADA-GHK group compared to ADA-Gel and ADA-Gel-GHK groups ($P < 0.001$). However, viability recovered in the ADA-GHK group reaching 96.4% at day 21, which was significantly higher than both in ADA-Gel and ADA-Gel-GHK groups ($P < 0.001$ & $P = 0.002$ respectively), as shown in Fig. 2A, C. Proliferation was higher in ADA-Gel-GHK compared to ADA-Gel and ADA-GHK groups at day 7 ($P < 0.001$) and 14 ($P < 0.01$). Nevertheless, at the final time point, both GHK-containing groups harbored significantly higher cell numbers than ADA-Gel ($P < 0.001$ & $P = 0.01$ for ADA-GHK & ADA-Gel-GHK, respectively), as shown in Fig. 2B. Even though no statistically significant difference in cell numbers was identified at day 21 between ADA-Gel-GHK and ADA-GHK hydrogels, it should be mentioned that viability was significantly lower in ADA-Gel-GHK compared to ADA-GHK.

3.3. GHK stimulates osteogenic differentiation

Osteogenic differentiation was assessed by analyzing ALP activity, FTIR spectra, bone extracellular matrix protein deposition and osteogenic gene expression. As shown in Fig. 3A, ADA-GHK

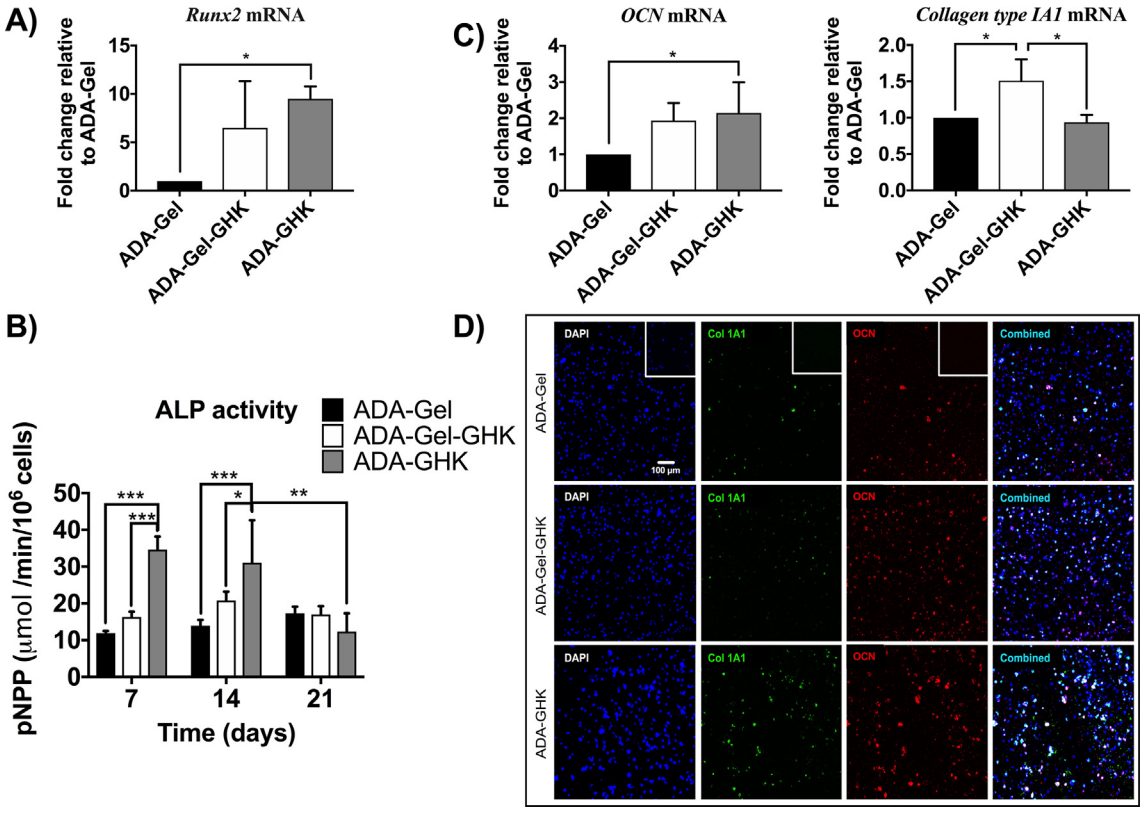

Fig. 3. Osteogenic differentiation of UCB MSCs in hydrogels Real time qRT-PCR analysis of *Runx2* prior to the chemical induction of osteogenesis (day 0 of differentiation) (A) as well as osteocalcin (OCN)/collagen 1A1 expression at day 21 of differentiation (C). ALP activity over 21 days of osteogenic differentiation (B). Immunofluorescence confocal microscopy evaluated the accumulation of Col 1A1 (green) and OCN at day 21 of differentiation (D). qRT-PCR results have been normalized to RPL13a as a reference gene and expressed as fold change relative to ADA-Gel; Bars represent mean ± SD (N = 3); Scale bar = 100 μm; Inserts represent negative controls for non-specific staining of the secondary antibody; * $P < 0.05$; ** $P < 0.01$; *** $P < 0.001$. (For interpretation of the references to color in this figure legend, the reader is referred to the web version of this article.)

Please cite this article as: M. E. Klontzas, S. Reakasame, R. Silva et al., Oxidized alginate hydrogels with the GHK peptide enhance cord blood mesenchymal stem cell osteogenesis: A paradigm for metabolomics-based evaluation of biomaterial design, Acta Biomaterialia, https://doi.org/10.1016/j.actbio.2019.02.017

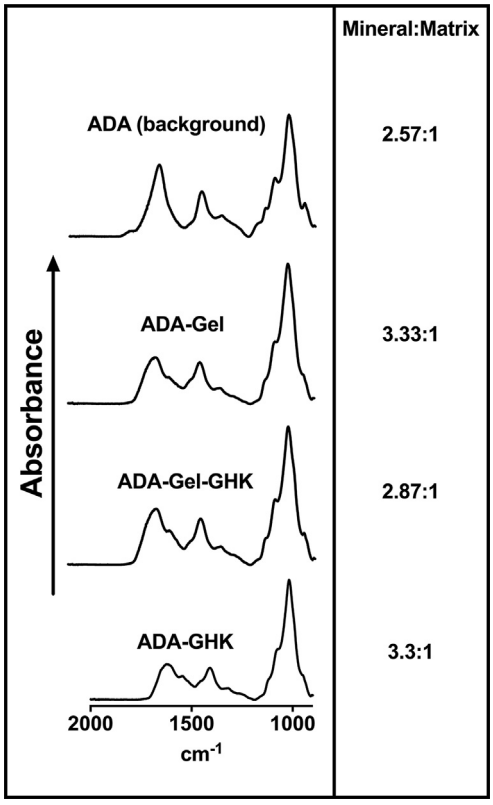

Fig. 4. Mineral:matrix ratios were calculated by dividing the area under the curve of phosphate bands (900–1200 cm^{-1}) by the area under the curve of amide I bands (1585–1725 cm^{-1}). FTIR absorbance measurements are provided on the left part, whereas corresponding mineral:matrix ratios are presented on the right part of the figure. The spectrum of ADA has been obtained as a background measurement in the absence of cells.

hydrogels achieved approximately 10-fold increase in *Runx2* mRNA levels, prior to the chemical induction of osteogenesis ($P = 0.041$), solely under the effect of the peptide, assuming that no other factors affecting the composition of our hydrogels are contributing to the phenomenon. During the early stages of differentiation, ALP activity was significantly higher in ADA-GHK hydrogels than in ADA-Gel (2.9-fold at day 7 and 2.22-fold at day 14 – $P < 0.001$) and ADA-Gel-GHK groups (2.12-fold at day 7 and 1.5-fold at day 14 – $P < 0.001$ & $P = 0.03$ for day 7 and day 14 respectively) as demonstrated in Fig. 3B. Only in ADA-GHK hydrogels, ALP activity significantly declined at day 21 compared to day 14 ($P = 0.004$).

At the final day of differentiation (day 21), *OCN* gene expression was significantly increased in the ADA-GHK group compared to the ADA-Gel group (2.4-fold; $P < 0.05$), whereas *Col IA1* gene expression was higher in ADA-Gel-GHK compared to both other groups (1.5-fold; $P = 0.02$ for both comparisons), as shown in Fig. 3C. These results were further corroborated by immunofluorescence microscopy, where deposition of OCN appeared higher in GHK-containing groups and Col IA1 deposition appeared higher in the ADA-GHK group (Fig. 3D). At the end of differentiation, the MM_r of ADA-Gel and ADA-GHK groups was approximately 3.3:1, compared to 2.87:1 of ADA-Gel-GHK and 2.57:1 of plain ADA (Fig. 4).

3.4. Metabolomics captures differentiation efficiency of ADA-GHK hydrogels

Metabolomics analysis was performed at days 0 and 21 of osteogenic differentiation and samples were compared to primary osteoblasts to assess the transition from undifferentiated to osteoblastic phenotype. As revealed by PCA (Fig. 5A and Supplementary Fig. 1), cells in gelatin-containing hydrogels (ADA-Gel & ADA-Gel-GHK) had greater variability in their metabolic profiles in comparison to ADA-GHK hydrogels, the profiles of which grouped closer to each other on principal component 1. In contrast, GHK-differentiated cells at the end of osteogenic differentiation

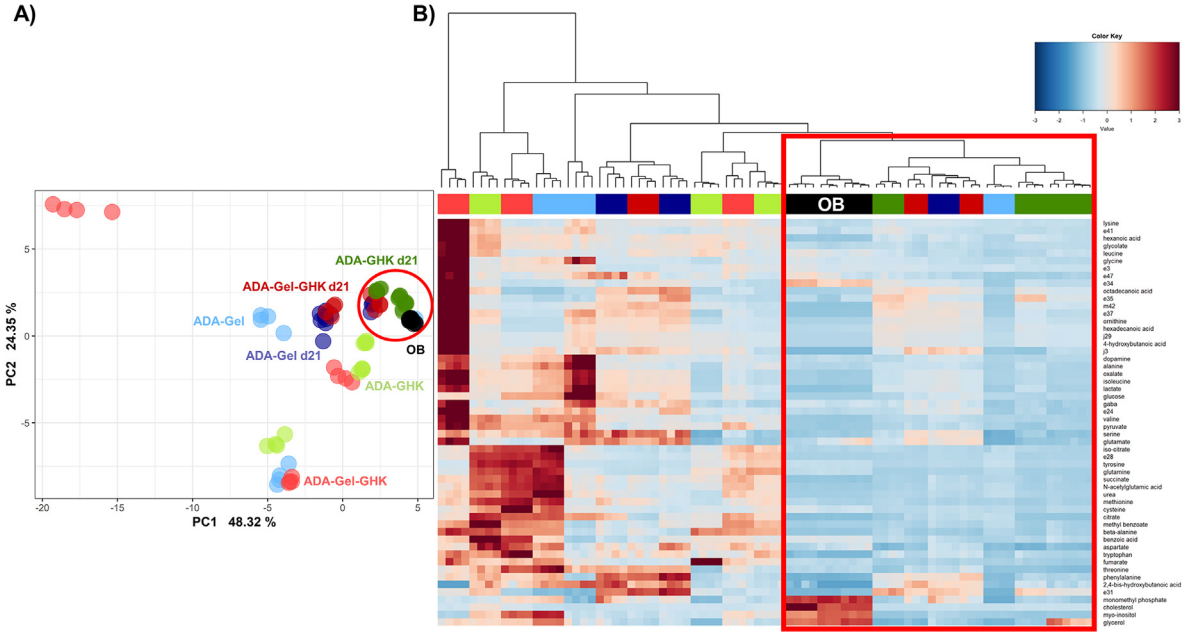

Fig. 5. Principal component analysis (A) and hierarchical clustering (B) of UCB MSC metabolomics profiles in hydrogels. PC1, PC2: percentage of variation described by principal component 1 and 2 respectively. Undifferentiated cells in ADA-Gel, ADA-Gel-GHK and ADA-GHK hydrogels are colored light blue, red and green respectively. Profiles of differentiated cells in ADA-Gel, ADA-Gel-GHK and ADA-GHK (day 21 – d21) are colored dark blue, red and green respectively whereas primary osteoblasts (OB) are colored black ($N = 3$ for each group). The red highlighted area demonstrates the cluster with osteoblasts and differentiated cells in GHK hydrogels. (For interpretation of the references to color in this figure legend, the reader is referred to the web version of this article.)

Please cite this article as: M. E. Klontzas, S. Reakasame, R. Silva et al., Oxidized alginate hydrogels with the GHK peptide enhance cord blood mesenchymal stem cell osteogenesis: A paradigm for metabolomics-based evaluation of biomaterial design, Acta Biomaterialia, https://doi.org/10.1016/j.actbio.2019.02.017

(day 21) displayed metabolic profiles grouped closer to osteoblasts than all other differentiated groups. These results were further supported by the HCl (Fig. 5B) whereby at day 21 all of the ADA-GHK and the majority of ADA-Gel-GHK profiles formed a common cluster with osteoblasts. This was not the case for day 21 ADA-Gel profiles, which clustered separately showing higher similarity to undifferentiated cells than osteoblasts. Importantly, metabolic activity in the osteoblast-containing cluster was globally less active than the activity of undifferentiated UCB MSCs.

On-network significance analysis revealed distinct metabolic transitions when comparing undifferentiated to terminally differentiated cells in various hydrogels (Fig. 6). Transitioning from day 0 to day 21 of differentiation, the activity of glycolysis, TCA cycle, glutaminolysis and urea cycle was reduced in all groups, as shown by the significant reduction in the levels of glucose, pyruvate, TCA cycle intermediates (citrate, isocitrate, succinate, fumarate), glutamine, urea, and N-acetylglutamic acid. The activity of glutaminolysis was increased in ADA-Gel and decreased in the ADA-GHK group. In ADA-Gel hydrogels, cholesterol levels were increased whereas glycine catabolism and oxalate synthesis were reduced compared to undifferentiated cells, changes that were absent in both GHK-containing hydrogels.

Cells in ADA-GHK hydrogels had minimal metabolic differences compared to osteoblasts, as shown by the limited number of significantly different metabolites between terminally-differentiated (day 21) cells and osteoblasts (Fig. 6). Specifically, osteoblasts had higher levels of lipids and lipid precursors, such as cholesterol and myo-inositol, as well as amino acids, such as glutamine, threonine, aspartate and tyrosine). In contrast, both ADA-Gel and ADA-Gel-GHK groups had higher lipids (hexadecanoic and octadecanoic acid) and lower lipid precursors (glycerol, myo-inositol) than osteoblasts, and higher amino acid pools, as well as higher glycolytic activity and lactate production. However, TCA cycle activity of gelatin-containing hydrogels was similar to osteoblasts.

Given the fact that UCB MSC metabolism may have been affected by the differences in hydrogel composition prior to differentiation, comparisons were also performed between hydrogel groups prior to the initiation of osteogenesis. As seen in Fig. 7 cells in ADA-GHK hydrogels had significantly higher levels of lipids (octadecanoic and cholesterol), fumarate and aminoacids (β-

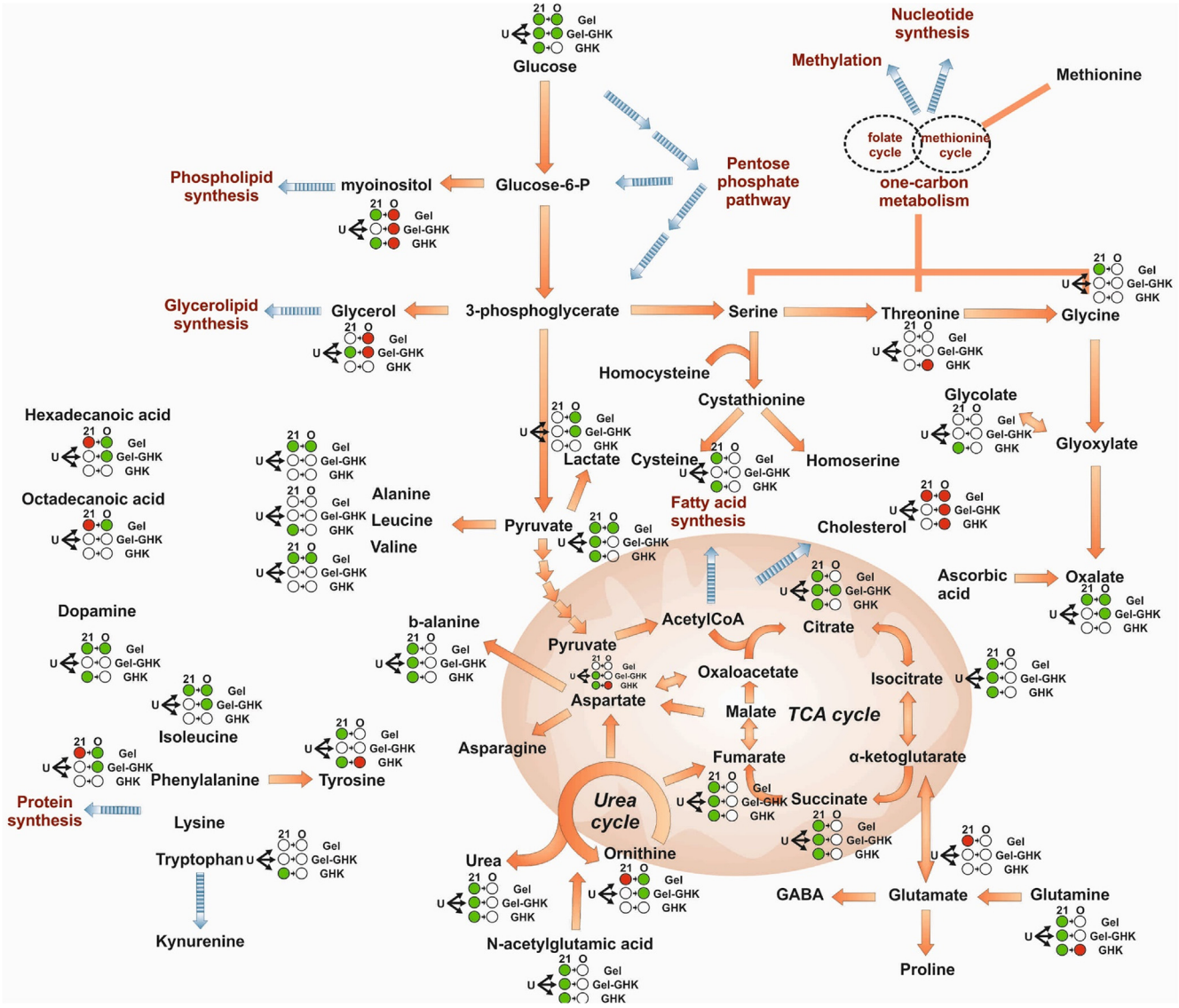

Fig. 6. On-network significance analysis of metabolic changes in UCB MSCs differentiated in hydrogels. Red circles and green circles denote a significant increase or decrease respectively, compared to the previous time point/condition. White circles were used when no significant change was seen with respect to the previous time point/condition. U: undifferentiated UCB MSCs in the respective hydrogel; 21: day 21 of differentiation; Gel: ADA-Gel; Gel-GHK: ADA-Gel-GHK; GHK: ADA-GHK; O: osteoblasts. (For interpretation of the references to color in this figure legend, the reader is referred to the web version of this article.)

Please cite this article as: M. E. Klontzas, S. Reakasame, R. Silva et al., Oxidized alginate hydrogels with the GHK peptide enhance cord blood mesenchymal stem cell osteogenesis: A paradigm for metabolomics-based evaluation of biomaterial design, Acta Biomaterialia, https://doi.org/10.1016/j.actbio.2019.02.017

alanine, aspartate, tryptophan and leucine), lower glycolytic activity and lactate production than cells in ADA-Gel hydrogels. In addition, the activity of serine-threonine-glycine pathway, glutaminolysis and amino acid pool levels were lower in the ADA-GHK compared to ADA-Gel groups. Interestingly, when comparing ADA-GHK to ADA-Gel-GHK hydrogels the differences were similar apart from the increase in lipids/lipid precursors and amino acids (Fig. 8). Finally, the activity of glycolysis, glutaminolysis and the levels of lipid precursors (glycerol, myo-inositol and citrate) were lower in ADA-Gel-GHK than in ADA-Gel hydrogels (Fig. 9). Similar comparisons between groups were performed at day 21. Cells in ADA-GHK hydrogels had lower glycolytic and glutaminolytic activity, decreased amino acid pools and lower levels of one-carbon cycle intermediates compared to cells in ADA-Gel hydrogels (Fig. 10). Comparable differences were observed between ADA-GHK and ADA-Gel-GHK hydrogels (Fig. 11). Comparison of ADA-Gel-GHK and ADA-Gel groups showed lower glycolysis, glutaminolysis, lipids/lipid precursors (glycerol, myo-inositol, citrate, cholesterol) and decreased amino acid pools in ADA-Gel-GHK hydrogels (Fig. 12).

3.5. ILK mediates the actions of GHK

The hypothesis that ILK mediates the effects of GHK in ADA-based hydrogels was evaluated by assessing ILK and integrin β1 mRNA and protein levels and by inhibiting the action of ILK with the use of CPD22, a specific and potent ILK inhibitor. Immunofluorescence confirming the presence of integrin β1 and ILK in undifferentiated cells at the start of the differentiation period (day 0), appeared to shower higher protein levels of ILK and integrin β1 in the ADA-GHK group compared to both ADA-Gel and ADA-Gel-GHK (Fig. 13A). Additionally, both *integrin β1* and *ILK* gene expression was significantly upregulated compared to ADA-Gel group at the start of differentiation (day 0; P = 0.041 & P = 0.0398 for integrin β1 & ILK, respectively), as shown in Fig. 13B, C. Inhibition of ILK with CPD22 did not affect cell viability (Fig. 14A). However, at day 3, ADA-GHK hydrogels had significantly higher cell numbers than plain ADA gels (approximately 1.4-fold higher, P = 0.004), an effect which was reversed when ILK was inhibited by CPD22 (P = 0.01), as shown in Fig. 14A Similarly, PCA and HCl demonstrated that UCB MSC metabolism changed due to GHK but the effect was reversed

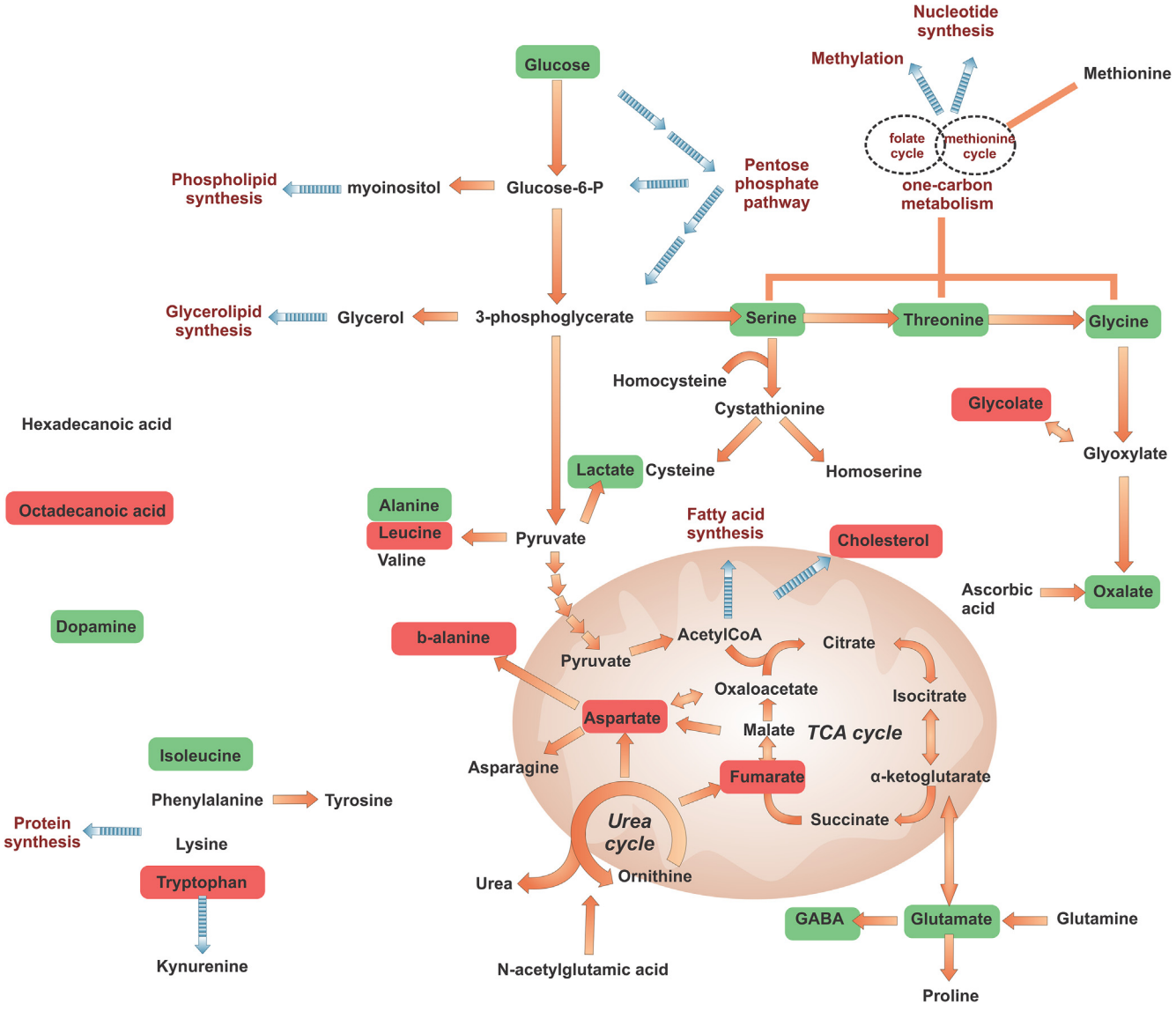

Fig. 7. On-network significance comparison between undifferentiated cells in ADA-GHK and ADA-Gel hydrogels. Green and red color denote significantly lower and higher metabolite level respectively, in the first of the two groups compared. (For interpretation of the references to color in this figure legend, the reader is referred to the web version of this article.)

Please cite this article as: M. E. Klontzas, S. Reakasame, R. Silva et al., Oxidized alginate hydrogels with the GHK peptide enhance cord blood mesenchymal stem cell osteogenesis: A paradigm for metabolomics-based evaluation of biomaterial design, Acta Biomaterialia, https://doi.org/10.1016/j.actbio.2019.02.017

with the application of CPD22 (Fig. 14B, C and Supplementary Fig. 2), confirming that activation of ILK by GHK did not only affect proliferation but also metabolism of UCB MSCs (Fig. 14D).

4. Discussion

Herein, global metabolomics signatures were utilized in the process of developing a novel ADA-based hydrogel containing the GHK peptide, which enhanced the proliferation, viability and osteogenic differentiation of UCB MSCs. Importantly, metabolomics verified the enhanced osteogenic efficiency of the ADA-GHK hydrogels, guiding the selection of biomaterials able to produce cells with high phenotypic reproducibility and similarity to osteoblasts, whilst providing valuable insight into the mechanism of GHK function. ADA-GHK hydrogels stimulated UCB MSC differentiation early (demonstrated by the early expression of *Runx2* in the absence of osteoinductive factors) and increased expression of late osteogenic markers compared to control gelatin-containing hydrogels, an effect that was successfully captured by metabolomics. Previous reports have shown that GHK can enhance fracture healing in animal models treated with gels composed of collagen, GHK and glucosaminoglycans [15], without providing a direct evaluation of the effect of GHK on MSC differentiation. Importantly, these *in vivo* results have been achieved with copper-free GHK, since copper inhibits MSC osteogenesis [54]. Previously, Jose et al. reported that alginate-copper-GHK hydrogels enhanced VEGF secretion from bone marrow MSCs [14], which could potentially serve the vasculogenic needs of bone regeneration and fracture repair [55]. Our study is the first to demonstrate that GHK can induce the osteogenic differentiation of MSCs.

Metabolomics captured the reduction in glycolytic and TCA cycle activity during osteogenic differentiation (in all groups), consistent with the well-reported transition from the glycolytic phenotype of undifferentiated MSCs to the production of energy by means of oxidative phosphorylation in differentiated cells [27,56,57]. However, comparison of the metabolism between the various hydrogel groups prior to the chemically-induced onset of osteogenic differentiation revealed lower glycolytic activity in the ADA-GHK compared to the ADA-Gel hydrogels, which given the significantly higher *Runx2* expression and early increase of ALP

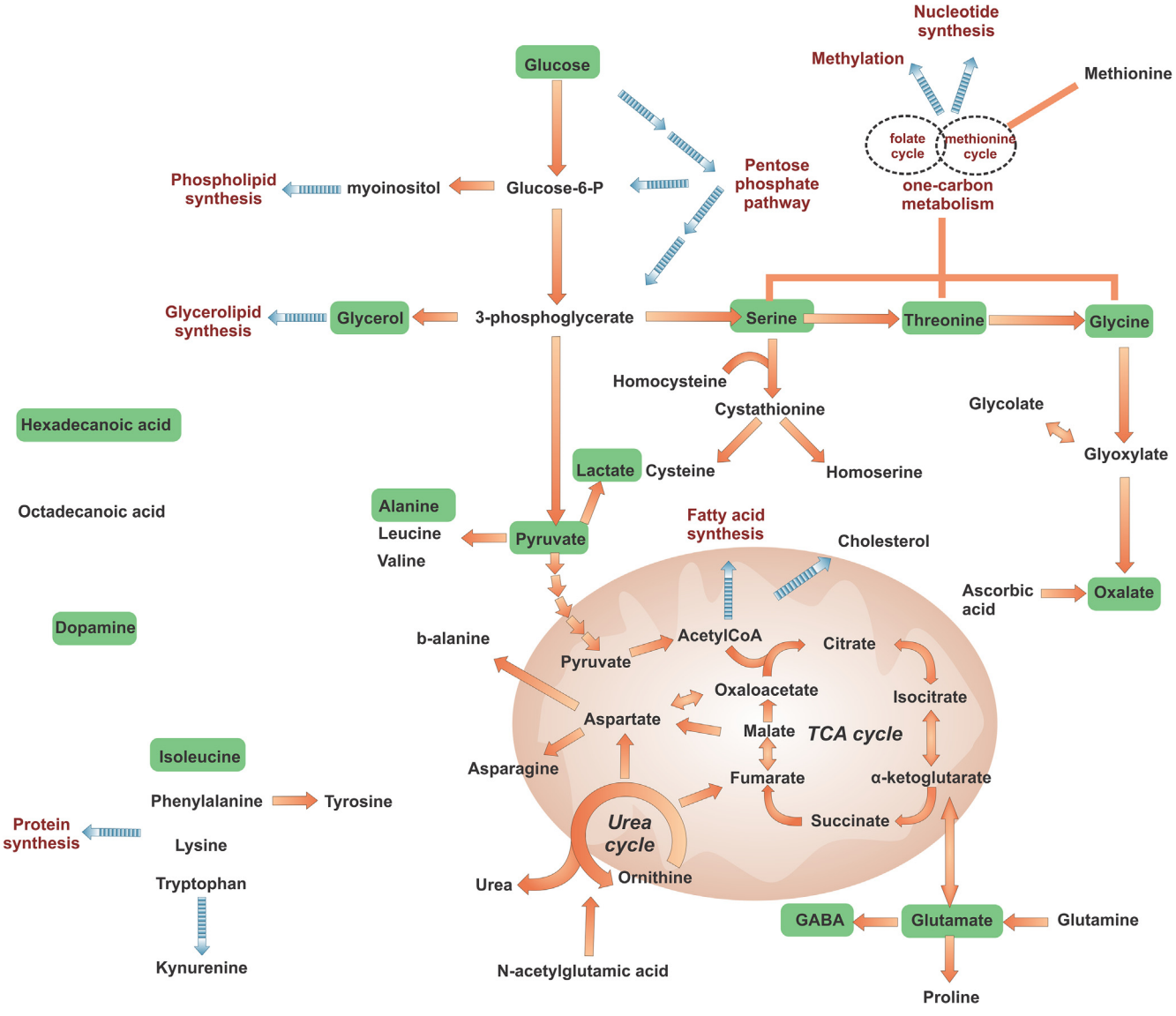

Fig. 8. On-network significance comparisons between undifferentiated cells in ADA-GHK and ADA-Gel-GHK hydrogels. Green and red color denote significantly lower and higher metabolite level respectively, in the first of the two groups compared. (For interpretation of the references to color in this figure legend, the reader is referred to the web version of this article.)

Please cite this article as: M. E. Klontzas, S. Reakasame, R. Silva et al., Oxidized alginate hydrogels with the GHK peptide enhance cord blood mesenchymal stem cell osteogenesis: A paradigm for metabolomics-based evaluation of biomaterial design, Acta Biomaterialia, https://doi.org/10.1016/j.actbio.2019.02.017

activity in cells exposed to GHK, signifies an earlier commitment towards the osteoblastic lineage. This early progression to osteogenic differentiation can be also related to the reduction in threonine and one-carbon metabolism precursors detected in the ADA-GHK group, which are required to maintain stemness [58]. The combination of more pronounced bone ECM production with higher *OCN* (late marker) and lower *Col IA1* gene expression (intermediate marker) in ADA-GHK hydrogels compared to gelatin-containing groups, indicate that GHK enhanced the progression from intermediate to late differentiation, which in our results was accompanied by lower glycolytic activity, in line with previous reports showing that glycolysis is reduced as osteogenesis progresses [27,56,57]. This is also indicated by the reduction of ALP activity in ADA-GHK hydrogels (day 21), which denotes progression to later differentiation stages [59,60]. In addition, increased levels of lipids and biosynthetic building blocks in the ADA-GHK group, can be attributed to increased activity of lipid-related signalling as well as active biosynthesis of molecules required for differentiation. Even though metabolomics has been previously used to identify molecules inducing osteogenesis in hydrogels of varying stiffness [28], to determine MSC responses to nanofeatured titania [30] and to evaluate the efficiency of osteoinductive substances in 2D cultures [27], our work is the first to demonstrate its application to the selection of biomaterials with desirable osteoinductive properties. Future *in vivo* experiments could further corroborate our results. Since metabolomics utilization herein proved to be a sensitive and robust assay for quality control of *in vitro* tissue engineering, metabolomics-guided *in vitro* validation of differentiation in biomaterials would facilitate the successful selection of optimal constructs for *in vivo* implantation. Prior to clinical use, animal studies are required to establish the absence of undifferentiated cells that may affect fracture healing.

ILK mediated the effect of GHK on UCB MSC proliferation and metabolism. Previous reports have shown that GHK binding to either integrin α_6, or β_1, or both can increase VEGF secretion [14] but our study was the first to demonstrate the involvement of ILK in GHK function. We observed increased expression of integrin $\beta 1$, in agreement with previously published data [14,61], but also identified the key intracellular mediator of GHK action. Integrin functions are predominantly mediated by focal adhesion kinase

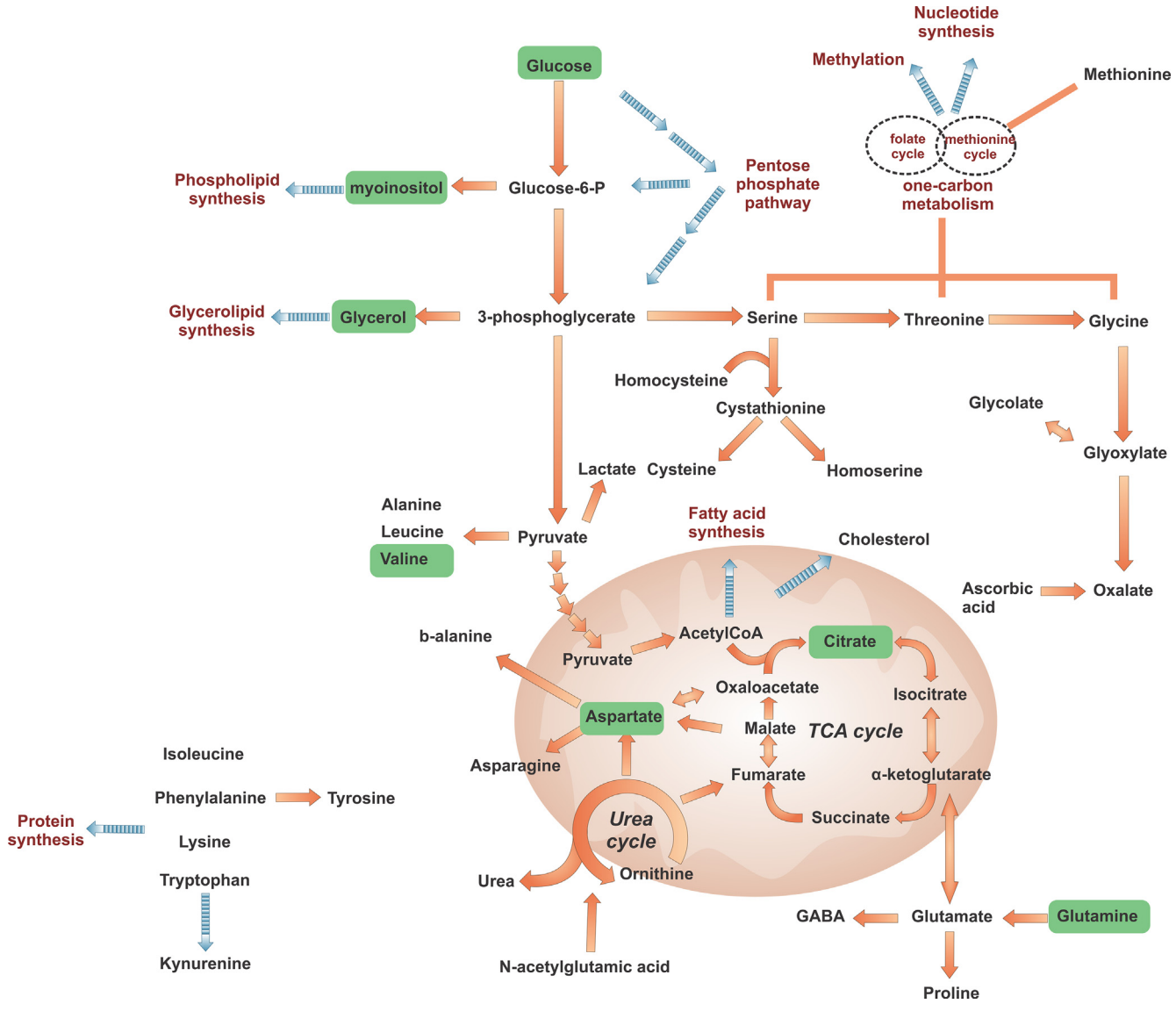

Fig. 9. On-network significance comparisons between undifferentiated cells in ADA-Gel-GHK and ADA-Gel hydrogels. Green and red color denote significantly lower and higher metabolite level respectively, in the first of the two groups compared. (For interpretation of the references to color in this figure legend, the reader is referred to the web version of this article.)

Please cite this article as: M. E. Klontzas, S. Reakasame, R. Silva et al., Oxidized alginate hydrogels with the GHK peptide enhance cord blood mesenchymal stem cell osteogenesis: A paradigm for metabolomics-based evaluation of biomaterial design, Acta Biomaterialia, https://doi.org/10.1016/j.actbio.2019.02.017

(FAK) and ILK [62]. These kinases control functions, including proliferation and migration, through the action of several pathways, such as the phosphatidylinositol 3-kinase (PI3K)-Akt-mTOR pathway, which also regulates lipid biosynthesis [63,64]. Acting upstream of FAK, ILK regulates its actions since ILK inhibition results to FAK dephosphorylation [65,66]. Despite the fact that FAK can independently activate downstream pathways related to metabolism, this is achieved in a delayed fashion compared to ILK [67]. We demonstrated that lipid biosynthesis was more pronounced in ADA-GHK compared to gelatin-containing hydrogels, and given the relationship between gelatin attachment and FAK activation [68], we hypothesized that GHK exerts its positive effects upstream of FAK via ILK. ILK involvement in GHK signalling is also supported by the fact that GHK is a fragment of SPARC, a well-established modulator of ILK activity [69]. Indeed, ILK mRNA and protein levels were higher in ADA-GHK hydrogels, whilst ILK inhibition eliminated the effect of GHK on proliferation and metabolism. Integrin binding can also explain the fact that ADA-Gel-GHK achieved higher differentiation than ADA-Gel alone but worse than ADA-GHK hydrogels, suggesting potential competition between gelatin and GHK. Gelatin binding to β1 receptors [70,71] could limit receptor availability for GHK, explaining the attenuated cellular response in ADA-Gel-GHK hydrogels. Our results indicate that various peptides/proteins induce differential metabolic results. Therefore, metabolomics could be further utilized to evaluate the effects of other peptides (e.g. RGD) on stem cell metabolism.

Unlike the uniform metabolism observed in the cells differentiated within the GHK-containing hydrogels, the metabolomics profiles of the cells from the gelatin-containing hydrogels were found to be variable at all stages of differentiation. Such heterogeneity could potentially be related to variations in size, shape and stiffness of the ADA-Gel and ADA-Gel-GHK hydrogels affecting mass transport of nutrients and metabolites as well as stem cell fate and metabolism [28,72–74]. However, within-group diameter variability in the generated hydrogels was low and comparable to the results in the seminal papers, which established the PBS-based ADA-Gel fabrication protocol [8] and showed that ADA-Gel hydrogels possess relatively consistent mechanical properties [10]. Consequently, metabolic variability in gelatin-containing hydrogels is more likely attributable to discrepancies in the availability of active gelatin binding sites. Indeed, Davidenko et al. showed that

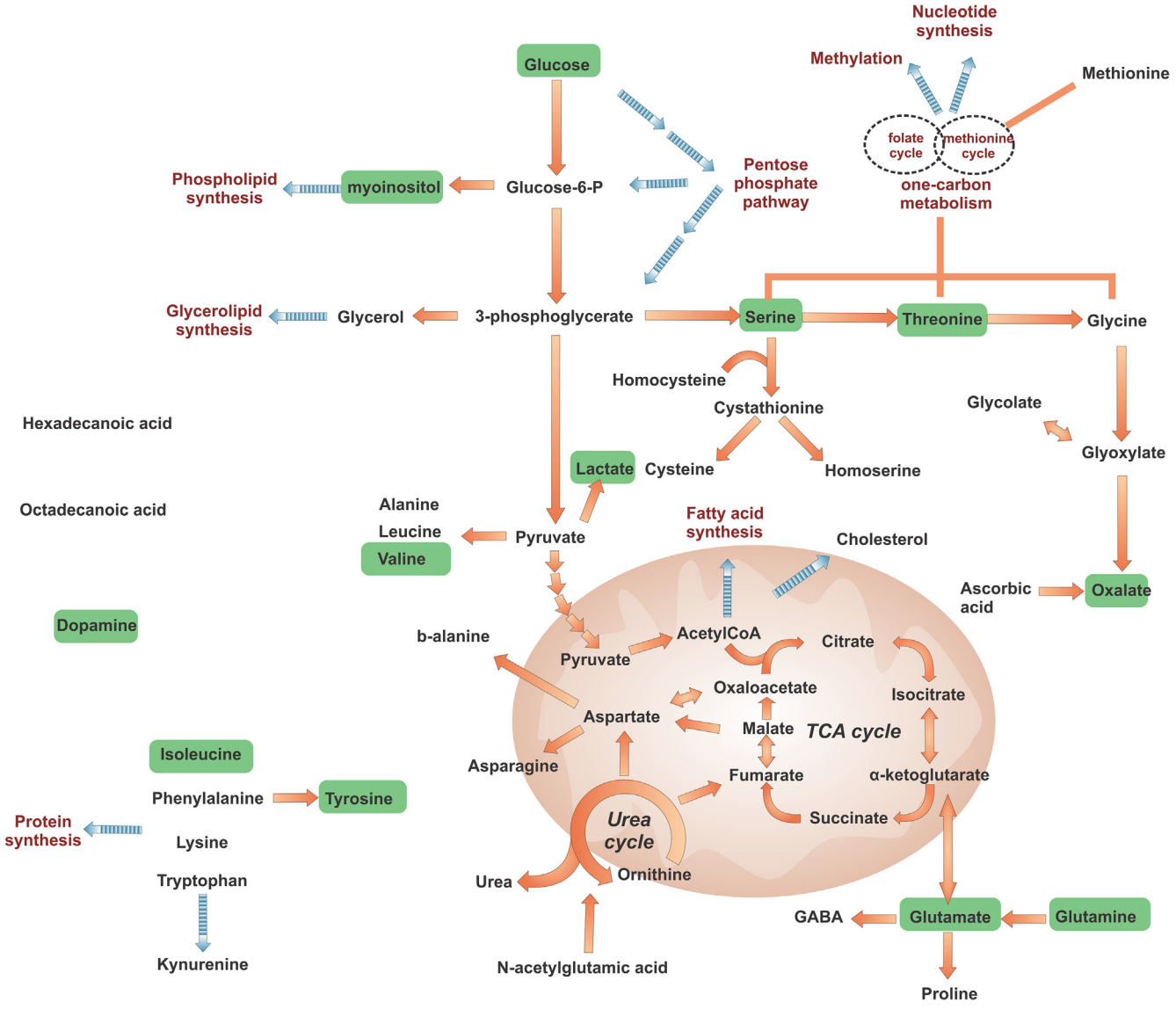

Fig. 10. On-network significance comparisons between terminally differentiated cells in ADA-GHK and ADA-Gel hydrogels (day 21). Green and red color denote significantly lower and higher metabolite level respectively, in the first of the two groups compared. (For interpretation of the references to color in this figure legend, the reader is referred to the web version of this article.)

Please cite this article as: M. E. Klontzas, S. Reakasame, R. Silva et al., Oxidized alginate hydrogels with the GHK peptide enhance cord blood mesenchymal stem cell osteogenesis: A paradigm for metabolomics-based evaluation of biomaterial design, Acta Biomaterialia, https://doi.org/10.1016/j.actbio.2019.02.017

crosslinking reduces integrin-dependent cell functions in 3D gelatin scaffolds, hampering experimental reproducibility [71]. As stated, metabolism was uniform in ADA-GHK hydrogels in contrast to the heterogeneous metabolism observed in the control gelatin hydrogels, highlighting the fact that metabolomics can assist in the selection of optimal biomaterials, ensuring the phenotypic reproducibility required for the clinical translation of cellular therapies.

Cells cultured in ADA-GHK hydrogels achieved the highest viability, amongst all groups, at the end of the differentiation process. This late recovery of viability in ADA-GHK may be responsible for the increase in proliferation noted at the end of the differentiation period. No significant degradation of the various hydrogel beads was observed during the culture period of 28 days, in contrast to pure ADA hydrogels, which could be attributed to the crosslinking between ADA and gelatine or GHK and is consistent with previous studies on the development of ADA-Gel hydrogels [8–11]. This reduced degradation rate could contribute to the rounded cell morphology observed in our results, which is in agreement with previous publications [75,76]. Other factors may also influence spreading of hydrogel encapsulated MSCs, such as gel relaxation, stiffness, the concentration of bioactive molecules and the availability and type of adhesive ligands [77,78]. Nonetheless, despite the rounded morphology cells still sufficiently differentiated to osteoblasts [76]. The smaller size of ADA-GHK beads (diameter around 2.3 mm) was comparable to previously published alginate-gelatin hydrogels where viability was reported to be high [79,80] allows for enhanced mass transport, including oxygen availability at the core, which would affect cell death [81]. In contrast, the larger ADA-Gel and ADA-Gel-GHK hydrogels (diameter around to 3 mm) experienced accumulation of cells at the periphery due to oxygen and nutrient transport limitations, which can result in dense ECM deposition on the outer surface of the beads, further hindering oxygen mass transport. Such differences in size, degradation rates and mechanical properties between pure ADA and ADA crosslinked with bioactive molecules [8,9], also render pure ADA unsuitable as a control for experiments where ADA has been functionalised with peptides and proteins. The presence of minuscule amounts of soluble GHK could be responsible for the initial reduction in cell viability in ADA-GHK, as evidenced by the

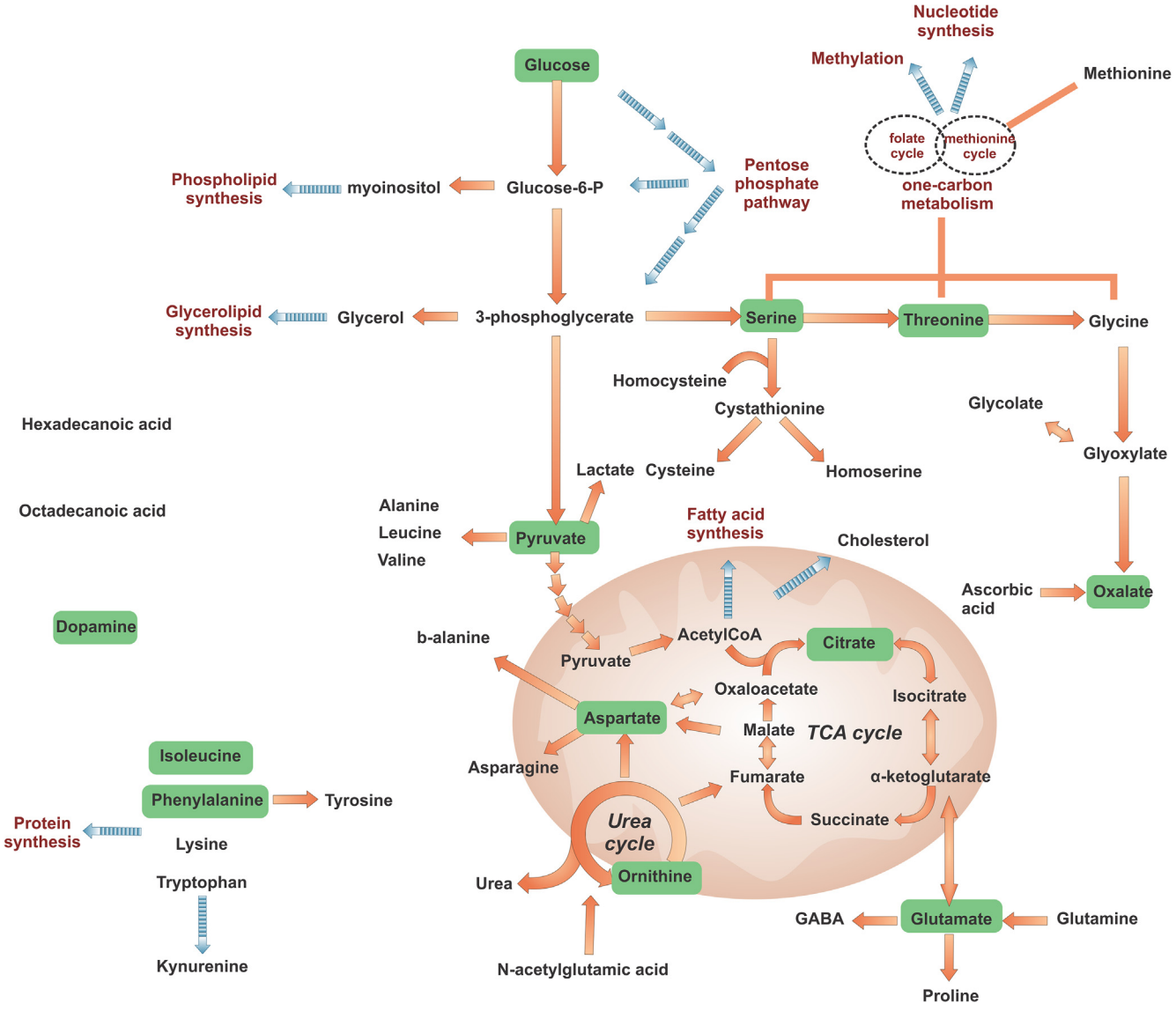

Fig. 11. On-network significance comparisons between terminally differentiated cells in ADA-GHK and ADA-Gel-GHK hydrogels (day 21). Green and red color denote significantly lower and higher metabolite level respectively, in the first of the two groups compared. (For interpretation of the references to color in this figure legend, the reader is referred to the web version of this article.)

Please cite this article as: M. E. Klontzas, S. Reakasame, R. Silva et al., Oxidized alginate hydrogels with the GHK peptide enhance cord blood mesenchymal stem cell osteogenesis: A paradigm for metabolomics-based evaluation of biomaterial design, Acta Biomaterialia, https://doi.org/10.1016/j.actbio.2019.02.017

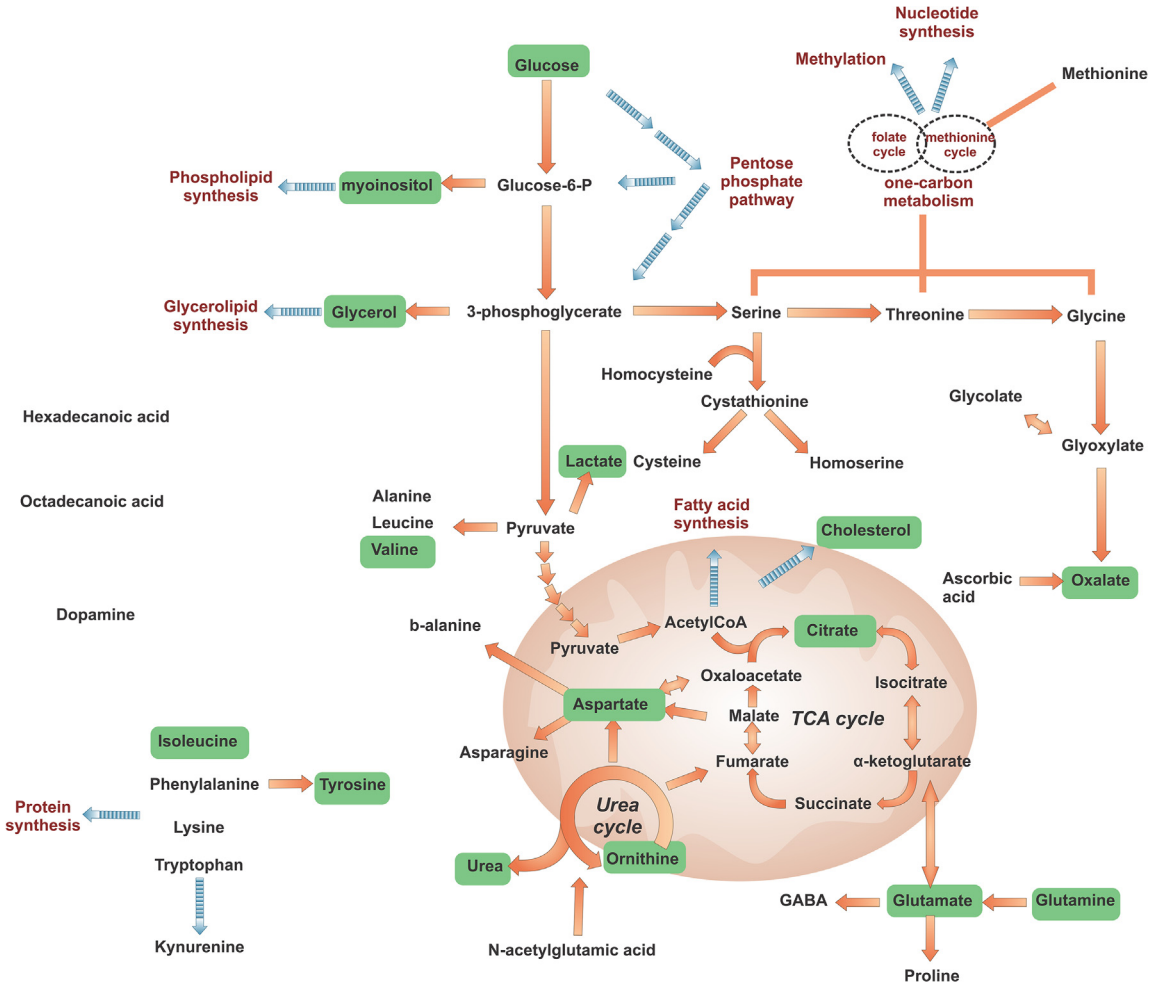

Fig. 12. On-network significance comparisons between terminally differentiated cells in ADA-Gel-GHK and ADA-Gel hydrogels (day 21). Green and red color denote significantly lower and higher metabolite level respectively, in the first of the two groups compared. (For interpretation of the references to color in this figure legend, the reader is referred to the web version of this article.)

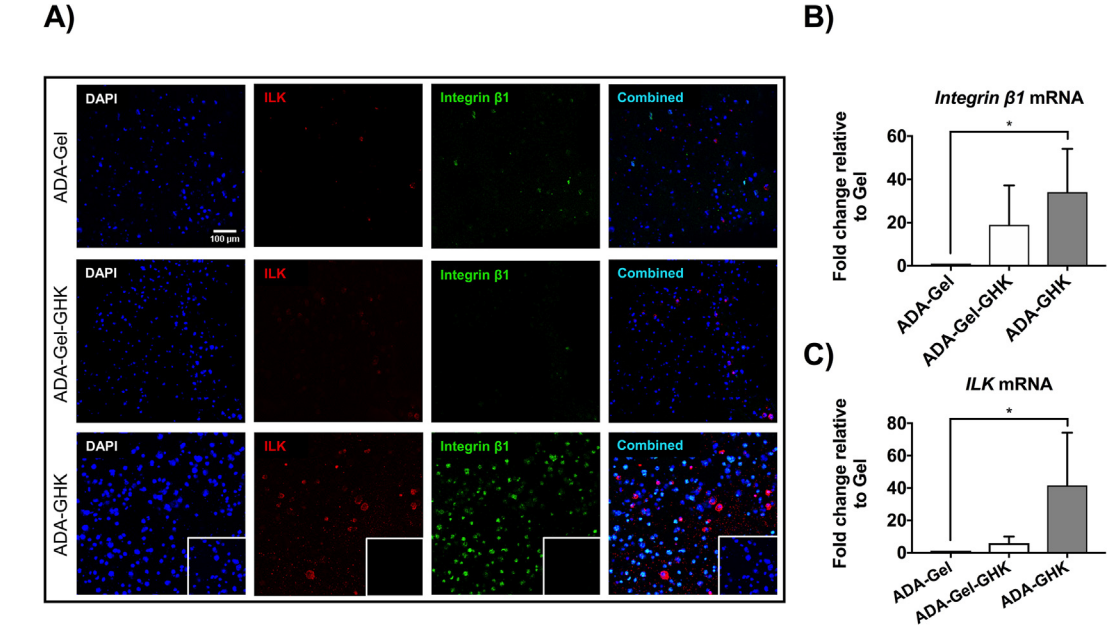

Fig. 13. ILK and integrin β1 protein and mRNA levels. Immunofluorescence confocal microscopy evaluated the presence of ILK (green) and integrin β1 prior to the initiation of osteogenesis (day 0) (A). Real time qRT-PCR analysis of *integrin β1 & ILK* prior to the initiation of osteogenesis (day 0) (B & C). qRT-PCR results have been normalized to RPL13a as a reference gene and expressed as fold change relative to ADA-Gel; Bars represent mean ± SD (N = 3); Scale bar = 100 μm; Inserts represent negative controls for non-specific staining of the secondary antibody. * $P < 0.05$. (For interpretation of the references to color in this figure legend, the reader is referred to the web version of this article.)

Please cite this article as: M. E. Klontzas, S. Reakasame, R. Silva et al., Oxidized alginate hydrogels with the GHK peptide enhance cord blood mesenchymal stem cell osteogenesis: A paradigm for metabolomics-based evaluation of biomaterial design, Acta Biomaterialia, https://doi.org/10.1016/j.actbio.2019.02.017

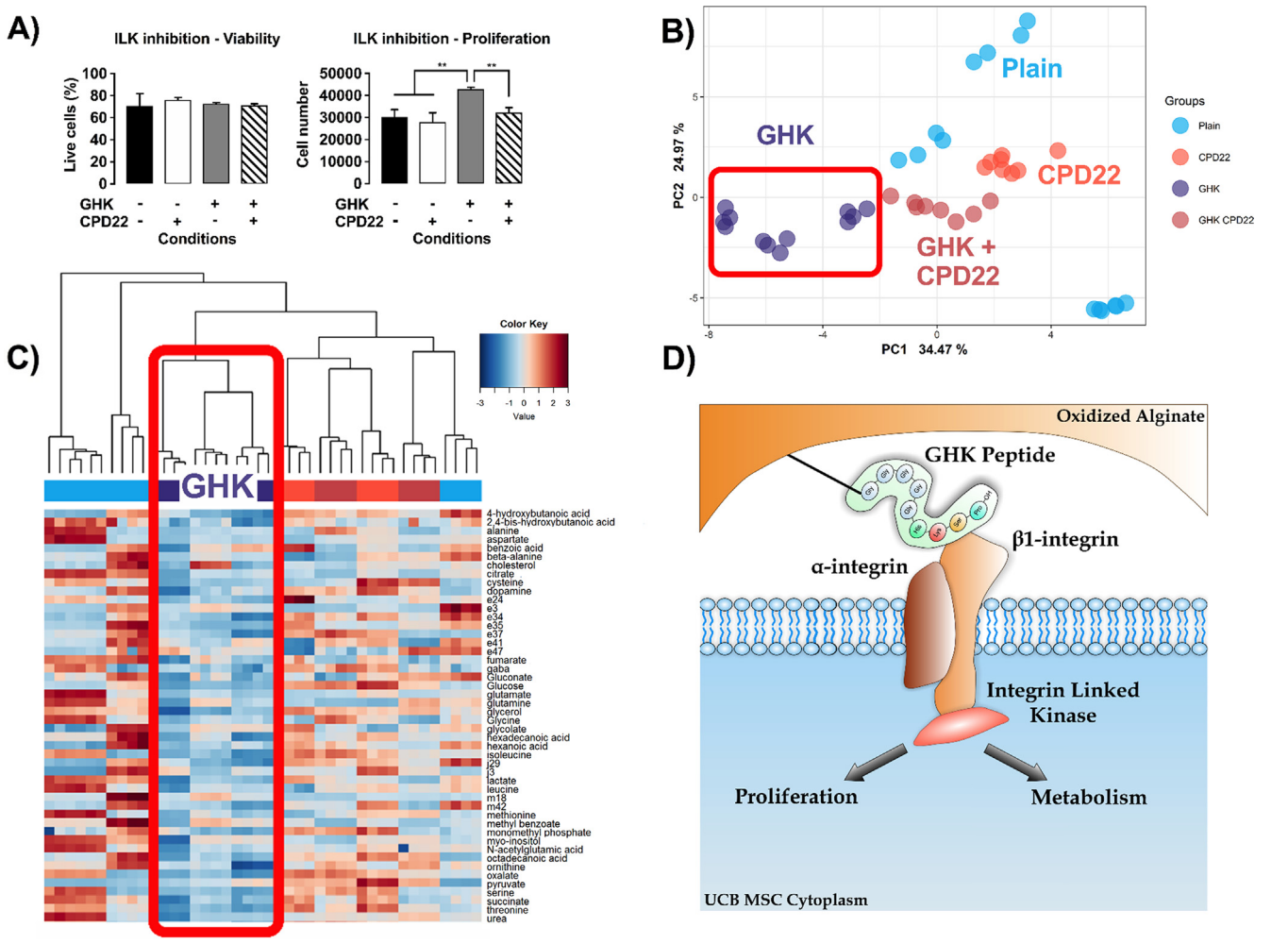

Fig. 14. Mechanism of GHK effect on UCB MSCs. Viability and proliferation (A) 48 h following the application of CPD22 (1 μM) (N = 3). Principal component analysis (B) and hierarchical clustering (C) of metabolomics profiles at 48 h after the application of CPD22 (N = 2–3). The highlighted red areas demonstrate the difference between ADA-GHK and plain ADA profiles which is eliminated with the application of CPD22. Proposed mechanism of GHK action in ADA hydrogels (D). Bars represent mean ± SD. ** $P < 0.01$; GHK: ADA-GHK. (For interpretation of the references to color in this figure legend, the reader is referred to the web version of this article.)

GHK release analysis. Indeed, it has been established that soluble integrin ligands can induce apoptosis whilst the same signal can maintain cell viability if bound to the ECM [82,83]. A limitation of our approach is the absence of scrambled GHK as experimental control. Prior to the use of such a control, its lack of bioactivity needs to be determined, since it could present a confounding factor affecting cellular metabolism.

In conclusion, novel ADA-GHK hydrogels have been produced that enhanced viability, proliferation and osteogenic differentiation of UCB MSCs, making them suitable for bone tissue engineering applications. In addition, metabolomics was used as a sensitive and robust validation and quality control tool in cell-based biomaterial development providing a mechanistic insight into the function of the biomaterial.

Declaration of interests

No conflict of interest to declare.

Data availability

Data used in this manuscript are available from authors upon reasonable request.

Acknowledgments

This work has received funding from the European Union's Horizon 2020 SymBioSys ITN (grant agreement no. 675585) and ERC Advanced Grant BioBlood (grant agreement no. 340719). Authors would like to thank Dr Mark Allenby for the fruitful discussions on confocal microscopy. Contributions: M.E.K., M.H, E.T., N.P., A.R.B. and A.M. designed research; M.E.K, J.C.F.M and R.J.M. performed experiments; M.E.K. analysed data; S.R, R.S. and A.R.B. provided hydrogels and developed GHK functionalisation method; M.E.K. and S.V. developed and optimized GC-MS metabolomics method for hydrogels; M.E.K., N.P. and A.M. wrote the paper. All authors have reviewed and provided comments for the paper.

Appendix A. Supplementary data

Supplementary data to this article can be found online at https://doi.org/10.1016/j.actbio.2019.02.017.

References

[1] K.Y. Lee, D.J. Mooney, Alginate: properties and biomedical applications, Prog. Polym. Sci. 37 (2012) 106–126.
[2] M.A. Lawson, J.E. Barralet, L. Wang, R.M. Shelton, J.T. Triffitt, Adhesion and growth of bone marrow stromal cells on modified alginate hydrogels, Tissue Eng. 10 (2004) 1480–1491.

[3] L. Wang, J. Shansky, C. Borselli, D. Mooney, H. Vandenburgh, Design and fabrication of a biodegradable, covalently crosslinked shape-memory alginate scaffold for cell and growth factor delivery, Tissue Eng. Part A 18 (2012) 2000–2007.
[4] S. Reakasame, A.R. Boccaccini, Oxidized alginate-based hydrogels for tissue engineering applications: a review, Biomacromolecules 19 (2018) 3–21.
[5] B. Balakrishnan, M. Mohanty, A.C. Fernandez, P.V. Mohanan, A. Jayakrishnan, Evaluation of the effect of incorporation of dibutyryl cyclic adenosine monophosphate in an in situ-forming hydrogel wound dressing based on oxidized alginate and gelatin, Biomaterials 27 (2006) 1355–1361.
[6] B. Balakrishnan, A. Jayakrishnan, Self-cross-linking biopolymers as injectable in situ forming biodegradable scaffolds, Biomaterials 26 (2005) 3941–3951.
[7] U. Rottensteiner, B. Sarker, D. Heusinger, D. Dafinova, S.N. Rath, J.P. Beier, U. Kneser, R.E. Horch, R. Detsch, A.R. Boccaccini, A. Arkudas, In vitro and in vivo biocompatibility of alginate dialdehyde/gelatin hydrogels with and without nanoscaled bioactive glass for bone tissue engineering applications, Materials (Basel) 7 (2014) 1957–1974.
[8] B. Sarker, D.G. Papageorgiou, R. Silva, T. Zehnder, F. Gul-E-Noor, M. Bertmer, J. Kaschta, K. Chrissafis, R. Detsch, A.R. Boccaccini, Fabrication of alginate–gelatin crosslinked hydrogel microcapsules and evaluation of the microstructure and physico-chemical properties, J. Mater. Chem. B 2 (2014) 1470.
[9] A. Grigore, B. Sarker, B. Fabry, A.R. Boccaccini, R. Detsch, Behavior of encapsulated MG-63 cells in RGD and gelatine-modified alginate hydrogels, Tissue Eng. Part A 20 (2014) 2140–2150.
[10] B. Sarker, T. Zehnder, S.N. Rath, R.E. Horch, U. Kneser, R. Detsch, A.R. Boccaccini, Oxidized alginate-gelatin hydrogel: a favorable matrix for growth and osteogenic differentiation of adipose-derived stem cells in 3D, ACS Biomater. Sci. Eng. 3 (2017) 1730–1737.
[11] T. Zehnder, B. Sarker, A.R. Boccaccini, R. Detsch, Evaluation of an alginate-gelatine crosslinked hydrogel for bioplotting, Biofabrication. 7 (2015) 025001.
[12] B. Wright, P.A. De Bank, K.A. Luetchford, F.R. Acosta, C.J. Connon, Oxidized alginate hydrogels as niche environments for corneal epithelial cells, J. Biomed. Mater. Res. A 102 (2014) 3393–3400.
[13] H.F. Ahmad, A. Sambanis, Cryopreservation effects on recombinant myoblasts encapsulated in adhesive alginate hydrogels, Acta Biomater. 9 (2013) 6814–6822.
[14] S. Jose, M.L. Hughbanks, B.Y.K. Binder, G.C. Ingavle, J.K. Leach, Enhanced trophic factor secretion by mesenchymal stem/stromal cells with Glycine-Histidine-Lysine (GHK)-modified alginate hydrogels, Acta Biomater. 10 (2014) 1955–1964.
[15] H. Pohunková, J. Stehlík, J. Váchal, O. Čech, M. Adam, Morphological features of bone healing under the effect of collagen-graft-glycosaminoglycan copolymer supplemented with the tripeptide Gly-His-Lys, Biomaterials 17 (1996) 1567–1574.
[16] L. Pickart, The human tri-peptide GHK and tissue remodeling, J. Biomed. Sci. Polym. Ed. 19 (2008) 969–988.
[17] D. Godet, P.J. Marie, Effects of the tripeptide glycyl-L-histidyl-L-lysine copper complex on osteoblastic cell spreading, attachment and phenotype, Cell. Mol. Biol. 41 (1995) 1081–1091.
[18] S. Kern, H. Eichler, J. Stoeve, H. Klüter, K. Bieback, Comparative analysis of mesenchymal stem cells from bone marrow, umbilical cord blood, or adipose tissue, Stem Cells 24 (2006) 1294–1301.
[19] G. Liu, Y. Li, J. Sun, H. Zhou, W. Zhang, L. Cui, Y. Cao, In vitro and in vivo evaluation of osteogenesis of human umbilical cord blood-derived mesenchymal stem cells on partially demineralized bone matrix, Tissue Eng. Part A 16 (2010) 971–982.
[20] M.E. Klontzas, E.I. Kenanidis, M. Heliotis, E. Tsiridis, A. Mantalaris, Bone and cartilage regeneration with the use of umbilical cord mesenchymal stem cells Bone and cartilage regeneration with the use of umbilical cord mesenchymal stem cells, Expert Opin. Biol. Ther. 15 (2015) 1541–1552.
[21] B. Sacchetti, A. Funari, C. Remoli, G. Giannicola, G. Kogler, S. Liedtke, G. Cossu, M. Serafini, M. Sampaolesi, E. Tagliafico, E. Tenedini, I. Saggio, P.G. Robey, M. Riminucci, P. Bianco, No identical "mesenchymal stem cells" at different times and sites: human committed progenitors of distinct origin and differentiation potential are incorporated as adventitial cells in microvessels, Stem Cell Rep. 6 (2016) 897–913.
[22] O. Fiehn, Metabolomics–the link between genotypes and phenotypes, Plant Mol. Biol. 48 (2002) 155–171.
[23] C.H. Johnson, J. Ivanisevic, G. Siuzdak, Metabolomics: beyond biomarkers and towards mechanisms, Nat. Rev. Mol. Cell Biol. 17 (2016) 451–459.
[24] S.I. Vernardis, C.T. Goudar, M.I. Klapa, Metabolic profiling reveals that time related physiological changes in mammalian cell perfusion cultures are bioreactor scale independent, Metab. Eng. 19 (2013) 1–9.
[25] S. Selvarasu, Y.S. Ho, W.P.K. Chong, N.S.C. Wong, F.N.K. Yusufi, Y.Y. Lee, M.G.S. Yap, D.Y. Lee, Combined in silico modeling and metabolomics analysis to characterize fed-batch CHO cell culture, Biotech. Bioeng. 109 (2012) 1415–1429.
[26] H. Kanani, P.K. Chrysanthopoulos, M.I. Klapa, Standardizing GC-MS metabolomics, J. Chromatogr. B 871 (2008) 191–201.
[27] M.E. Klontzas, S.I. Vernardis, M. Heliotis, E. Tsiridis, A. Mantalaris, Metabolomics analysis of the osteogenic differentiation of umbilical cord blood mesenchymal stem cells reveals differential sensitivity to osteogenic agents, Stem Cells Dev. 26 (2017) 723–733.
[28] E.V. Alakpa, V. Jayawarna, A. Lampel, K.V. Burgess, C.C. West, S.C.J. Bakker, S. Roy, N. Javid, S. Fleming, D.A. Lamprou, J. Yang, A. Miller, A.J. Urquhart, P.W.J.M. Frederix, N.T. Hunt, B. Péault, R.V. Ulijn, M.J. Dalby, Tunable supramolecular hydrogels for selection of lineage-guiding metabolites in stem cell cultures, Chemistry 1 (2016) 298–319.
[29] L.C.Y. Lee, N. Gadegaard, M.C. de Andrés, L.A. Turner, K.V. Burgess, S.J. Yarwood, J. Wells, M. Salmeron-Sanchez, D. Meek, R.O.C. Oreffo, M.J. Dalby, Nanotopography controls cell cycle changes involved with skeletal stem cell self-renewal and multipotency, Biomaterials 116 (2017) 10–20.
[30] L.E. McNamara, T. Sjöström, R.M.D. Meek, R.O.C. Oreffo, B. Su, M.J. Dalby, K.E.V. Burgess, Metabolomics: a valuable tool for stem cell monitoring in regenerative medicine, J. R. Soc. Interface 9 (2012) 1713–1724.
[31] A. Armiñán, M. Palomino-Schätzlein, C. Deladriere, J.J. Arroyo-Crespo, S. Vicente-Ruiz, M.J. Vicent, A. Pineda-Lucena, Metabolomics facilitates the discrimination of the specific anti-cancer effects of free- and polymer-conjugated doxorubicin in breast cancer models, Biomaterials 162 (2018) 144–153.
[32] S.I. Vernardis, K. Terzoudis, N. Panoskaltsis, A. Mantalaris, Human embryonic and induced pluripotent stem cells maintain phenotype but alter their metabolism after exposure to ROCK inhibitor, Sci. Rep. 7 (2017) 42138.
[33] P.K. Chrysanthopoulos, C.T. Goudar, M.I. Klapa, Metabolomics for high-resolution monitoring of the cellular physiological state in cell culture engineering, Metab. Eng. 12 (2010) 212–222.
[34] D. Sipp, P.G. Robey, L. Turner, Clear up this stem-cell mess, Nature 561 (2018) 455–457.
[35] S. Bolte, F.P. Cordelieres, A guided tour into subcellular colocalisation analysis in light microscopy, J. Microsc. 224 (2006) 213–232.
[36] J. Schindelin, I. Arganda-Carreras, E. Frise, V. Kaynig, M. Longair, T. Pietzsch, S. Preibisch, C. Rueden, S. Saalfeld, B. Schmid, J.-Y. Tinevez, D.J. White, V. Hartenstein, K. Eliceiri, P. Tomancak, A. Cardona, Fiji: an open-source platform for biological-image analysis, Nat. Meth. 9 (2012) 676–682.
[37] W.L. Grayson, M. Fröhlich, K. Yeager, S. Bhumiratana, M.E. Chan, C. Cannizzaro, L.Q. Wan, X.S. Liu, X.E. Guo, G. Vunjak-Novakovic, Engineering anatomically shaped human bone grafts, Proc. Natl. Acad. Sci. 107 (2010) 3299–3304.
[38] J.M. Karp, L.S. Ferreira, A. Khademhosseini, A.H. Kwon, J. Yeh, R.S. Langer, Cultivation of human embryonic stem cells without the embryoid body step enhances osteogenesis in vitro, Stem Cells 24 (2006) 835–843.
[39] D.A. Shimko, C.A. Burks, K.C. Dee, E.A. Nauman, Comparison of in vitro mineralization by murine embryonic and adult stem cells cultured in an osteogenic medium, Tissue Eng. 10 (2004) 1386–1398.
[40] E.P. Paschalis, F. Betts, E. DiCarlo, R. Mendelsohn, A.L. Boskey, FTIR microspectroscopic analysis of human iliac crest biopsies from untreated osteoporotic bone, Calcif. Tissue Int. 61 (1997) 487–492.
[41] K. Turksen, Stem Cell Nanotechnology: Methods and Protocols, Humana Press, Springer P, 2013.
[42] M.C. de Andrés, E. Kingham, K. Imagawa, A. Gonzalez, H.I. Roach, D.I. Wilson, R. O.C. Oreffo, Epigenetic regulation during fetal femur development: DNA methylation matters, PLoS One 8 (2013) e54957.
[43] S.H. Durand, V. Flacher, A. Roméas, F. Carrouel, E. Colomb, C. Vincent, H. Magloire, M.-L. Couble, F. Bleicher, M.-J. Staquet, S. Lebecque, J.-C. Farges, Lipoteichoic acid increases TLR and functional chemokine expression while reducing dentin formation in in vitro differentiated human odontoblasts, J. Immunol. 176 (2006) 2880–2887.
[44] D.H.K. Ma, H.C. Chen, K.S.K. Ma, J.Y. Lai, U. Yang, L.K. Yeh, Y.J. Hsueh, W.K. Chu, C.H. Lai, J.K. Chen, Preservation of human limbal epithelial progenitor cells on carbodiimide cross-linked amniotic membrane via integrin-linked kinase-mediated Wnt activation, Acta Biomater. 31 (2016) 144–155.
[45] G.Q. Felipe, O.M. Posada, D. Gallego-Perez, N. Higuita-Castro, C. Sarassa, D.J. Hansford, P. Agudelo-Florez, L.E. López, Housekeeping gene stability influences the quantification of osteogenic markers during stem cell differentiation to the osteogenic lineage, Cytotechnology 62 (2010) 109–120.
[46] D. Studer, S. Lischer, W. Jochum, M. Ehrbar, M. Zenobi-Wong, K. Maniura-Weber, Ribosomal protein L13a as a reference gene for human bone marrow-derived mesenchymal stromal cells during expansion, adipo-, chondro-, and osteogenesis, Tissue Eng. Part C 18 (2012) 761–771.
[47] K.J. Livak, T.D. Schmittgen, Analysis of relative gene expression data using real-time quantitative PCR and the $2-\Delta\Delta CT$ method, Methods 25 (2001) 402–408.
[48] L.P. Silva, P.L. Lorenzi, P. Purwaha, V. Yong, D.H. Hawke, J.N. Weinstein, Measurement of DNA concentration as a normalization strategy for metabolomic data from adherent cell lines, Anal. Chem. 85 (2013) 9536–9542.
[49] H.H. Kanani, M.I. Klapa, Data correction strategy for metabolomics analysis using gas chromatography–mass spectrometry, Metab. Eng. 9 (2007) 39–51.
[50] M.B. Eisen, P.T. Spellman, P.O. Brown, D. Botstein, Cluster analysis and display of genome-wide expression patterns, PNAS 95 (1998) 14863–14868.
[51] A.I. Saeed, V. Sharov, J. White, J. Li, W. Liang, N. Bhagabati, J. Braisted, M. Klapa, T. Currier, M. Thiagarajan, A. Sturn, M. Snuffin, A. Rezantsev, D. Popov, A. Ryltsov, E. Kostukovich, I. Borisovsky, Z. Liu, A. Vinsavich, V. Trush, J. Quackenbush, TM4: a free, open-source system for microarray data management and analysis, Biotechniques 34 (2003) 374–378.
[52] P. de la Puente, E. Weisberg, B. Muz, A. Nonami, M. Luderer, R.M. Stone, J.V. Melo, J.D. Griffin, A.K. Azab, Identification of ILK as a novel therapeutic target for acute and chronic myeloid leukemia, Leuk. Res. S0145–2126 (2015) 30377–30385.
[53] S.-L. Lee, E.-C. Hsu, C.-C. Chou, H.-C. Chuang, L.-Y. Bai, S.K. Kulp, C.-S. Chen, Identification and characterization of a novel integrin-linked kinase inhibitor, J. Med. Chem. 54 (2012) 6364–6374.
[54] S. Li, M. Wang, X. Chen, S.-F. Li, J. Li-Ling, H.-Q. Xie, Inhibition of osteogenic differentiation of mesenchymal stem cells by copper supplementation, Cell Prolif. 47 (2014) 81–90.

Please cite this article as: M. E. Klontzas, S. Reakasame, R. Silva et al., Oxidized alginate hydrogels with the GHK peptide enhance cord blood mesenchymal stem cell osteogenesis: A paradigm for metabolomics-based evaluation of biomaterial design, Acta Biomaterialia, https://doi.org/10.1016/j.actbio.2019.02.017

[55] M.E. Klontzas, E.I. Kenanidis, R.J. MacFarlane, T. Michail, M.E. Potoupnis, M. Heliotis, A. Mantalaris, E. Tsiridis, Investigational drugs for fracture healing: preclinical & clinical data, Exp. Opin. Invest Drugs 25 (2016).
[56] C.-T. Chen, Y.-R.V. Shih, T.K. Kuo, O.K. Lee, Y.-H. Wei, Coordinated changes of mitochondrial biogenesis and antioxidant enzymes during osteogenic differentiation of human mesenchymal stem cells, Stem Cells 26 (2008) 960–968.
[57] G. Pattappa, H.K. Heywood, J.D. de Bruijn, D.A. Lee, The metabolism of human mesenchymal stem cells during proliferation and differentiation, J. Cell. Physiol. 226 (2011) 2562–2570.
[58] J. Wang, P. Alexander, L. Wu, R. Hammer, O. Cleaver, S.L. McKnight, Dependence of mouse embryonic stem cells on threonine catabolism, Science (80-) 325 (2009) 435–439.
[59] J.E. Aubin, Regulation of osteoblast formation and function, Rev. Endocr. Metab. Disord. 2 (2001) 81–94.
[60] R.A. Thibault, L. Scott Baggett, A.G. Mikos, F.K. Kasper, Osteogenic differentiation of mesenchymal stem cells on pregenerated extracellular matrix scaffolds in the absence of osteogenic cell culture supplements, Tissue Eng. Part A 16 (2010) 431–440.
[61] H.R. Choi, Y.A. Kang, S.J. Ryoo, J.W. Shin, J.I. Na, C.H. Huh, K.C. Park, Stem cell recovering effect of copper-free GHK in skin, J. Pept. Sci. 18 (2012) 685–690.
[62] D.S. Harburger, D.A. Calderwood, Integrin signalling at a glance, J. Cell Sci. 122 (2009) 159–163.
[63] D.D. Liu, C.C. Han, H.F. Wan, F. He, H.Y. Xu, S.H. Wei, X.H. Du, F. Xu, Effects of inhibiting PI3K-Akt-mTOR pathway on lipid metabolism homeostasis in goose primary hepatocytes, Animal 10 (2016) 1319–1327.
[64] C.F. Yen, H.S. Wang, C.L. Lee, S.K. Liao, Roles of integrin-linked kinase in cell signaling and its perspectives as a therapeutic target, Gynecol. Minim. Invasive Ther. 3 (2014) 67–72.
[65] L. Vitillo, S.J. Kimber, Integrin and FAK regulation of human pluripotent stem cells, Curr. Stem Cell Rep. 3 (2017) 358–365.
[66] P.J. Wrighton, J.R. Klim, B.A. Hernandez, C.H. Koonce, T.J. Kamp, L.L. Kiessling, Signals from the surface modulate differentiation of human pluripotent stem cells through glycosaminoglycans and integrins, PNAS 111 (2014) 18126–18131.
[67] S. Dedhar, B. Williams, G. Hannigan, Integrin-linked kinase (ILK): a regulator of integrin and growth-factor signalling, Trends Cell Biol. 9 (1999) 319–323.
[68] A. Krouwels, F.P.W. Melchels, M.H.P. van Rijen, C.B.M. Ten Brink, W.J.A. Dhert, F. Cumhur Öner, M.A. Tryfonidou, L.B. Creemers, Focal adhesion signaling affects regeneration by human nucleus pulposus cells in collagen- but not carbohydrate-based hydrogels, Acta Biomater. 66 (2018) 238–247.
[69] T.H. Barker, G. Baneyx, M. Cardó-Vila, G.A. Workman, M. Weaver, P.M. Menon, S. Dedhar, S.A. Rempel, W. Arap, R. Pasqualini, V. Vogel, E.H. Sage, SPARC regulates extracellular matrix organization through its modulation of integrin-linked kinase activity, J. Biol. Chem. 280 (2005) 36483–36493.
[70] J.T. Elliott, J.T. Woodward, K.J. Langenbach, A. Tona, P.L. Jones, A.L. Plant, Vascular smooth muscle cell response on thin films of collagen, Matrix Biol. 24 (2005) 489–502.
[71] N. Davidenko, C.F. Schuster, D.V. Bax, R.W. Farndale, S. Hamaia, S.M. Best, R.E. Cameron, Evaluation of cell binding to collagen and gelatin: a study of the effect of 2D and 3D architecture and surface chemistry, J. Mater. Sci. – Mater. Med. 27 (2016) 148.
[72] D.F. Duarte Campos, A. Blaeser, A. Korsten, S. Neuss, J. Jäkel, M. Vogt, H. Fischer, The stiffness and structure of three-dimensional printed hydrogels direct the differentiation of mesenchymal stromal cells toward adipogenic and osteogenic lineages, Tissue Eng. Part A 21 (2015) 740–756.
[73] M. Guvendiren, J.A. Burdick, The control of stem cell morphology and differentiation by hydrogel surface wrinkles, Biomaterials 31 (2010) 6511–6518.
[74] W.-T. Hsieh, Y.-S. Liu, Y. Lee, M.G. Rimando, K. Lin, O.K. Lee, Matrix dimensionality and stiffness cooperatively regulate osteogenesis of mesenchymal stromal cells, Acta Biomater. 32 (2016) 210–222.
[75] S.A. Ferreira, P.A. Faull, A.J. Seymour, T.T. Yu, S. Loaiza, H.W. Auner, A.P. Snijders, E. Gentleman, Neighboring cells override 3D hydrogel matrix cues to drive human MSC quiescence, Biomaterials 176 (2018) 13–23.
[76] S.A. Ferreira, M.S. Motwani, P.A. Faull, A.J. Seymour, T.T. Yu, M. Enayati, D.K. Taheem, C. Salzlechner, T. Haghighi, E.M. Kania, O.P. Oommen, T. Ahmed, S. Loaiza, K. Parzych, F. Dazzi, O.P. Varghese, F. Festy, A.E. Grigoriadis, H.W. Auner, A.P. Snijders, L. Bozec, E. Gentleman, Bi-directional cell-pericellular matrix interactions direct stem cell fate, Nat. Commun. 9 (2018) 4049.
[77] S.R. Caliari, J.A. Burdick, A practical guide to hydrogels for cell culture, Nat. Meth. 13 (2016) 405–414.
[78] O. Chaudhuri, L. Gu, D. Klumpers, M. Darnell, S.A. Bencherif, J.C. Weaver, N. Huebsch, H.-P. Lee, E. Lippens, G.N. Duda, D.J. Mooney, Hydrogels with tunable stress relaxation regulate stem cell fate and activity, Nat. Mater. 15 (2010) 326–334.
[79] J. Zhang, M. Wang, J.M. Cha, A. Mantalaris, The incorporation of 70s bioactive glass to the osteogenic differentiation of murine embryonic stem cells in 3D bioreactors, J. Tissue Eng. Regen. Med. 3 (2009) 63–71.
[80] Y.-S. Hwang, J. Cho, F. Tay, J.Y.Y. Heng, R. Ho, S.G. Kazarian, D.R. Williams, A.R. Boccaccini, J.M. Polak, A. Mantalaris, The use of murine embryonic stem cells, alginate encapsulation, and rotary microgravity bioreactor in bone tissue engineering, Biomaterials 30 (2009) 499–507.
[81] C. McKee, G.R. Chaudhry, Advances and challenges in stem cell culture, Coll. Surf. B Biointerfaces 159 (2017) 62–77.
[82] D.G. Stupack, D.A. Cheresh, Apoptotic cues from the extracellular matrix: regulators of angiogenesis, Oncogene 22 (2003) 9022–9029.
[83] A. Tahlawi, M.E. Klontzas, M.C. Allenby, J.C.F. Morais, N. Panoskaltsis, A. Mantalaris, RGD-functionalized polyurethane scaffolds promote umbilical cord blood mesenchymal stem cell expansion and osteogenic differentiation, J. Tissue Eng. Regen. Med. (2018), https://doi.org/10.1002/term.2784.

Please cite this article as: M. E. Klontzas, S. Reakasame, R. Silva et al., Oxidized alginate hydrogels with the GHK peptide enhance cord blood mesenchymal stem cell osteogenesis: A paradigm for metabolomics-based evaluation of biomaterial design, Acta Biomaterialia, https://doi.org/10.1016/j.actbio.2019.02.017